Aalborg University

Energy Department

# Sensitivity Analysis of MTDC Control System

Long Master Thesis

Aalborg 2016

Przemyslaw Drozd

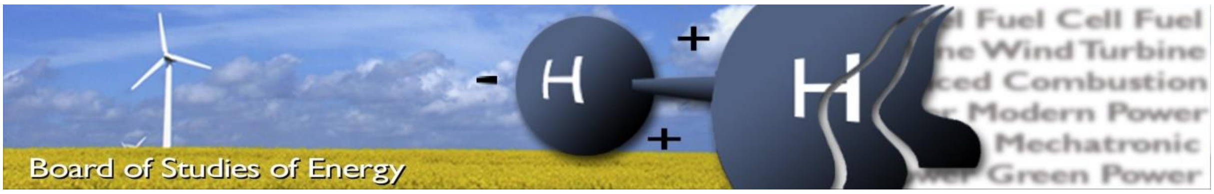


**Title: Sensitivity Analysis of MTDC Control System**

**Semester: 4th M.SC**

**Project period: 25.05.2016 – 25.08.2016**

**ECTS: 50**

**Supervisors: Filipe Faria da Silva**
**Roni Irnawan**

Copies: [Only digital version]

Pages, total: [73]

Appendix: [1]

**I confirm that I am liable for the contents of the report. Furthermore, I confirm that the report does not include plagiarism.**

# Abstract

The North Sea Offshore grid idea has been evaluated as one of a key structures, necessary to ensure the stability of supply in countries of European Union and reduce the energy imported from outside EU. The HVDC connection COBRAcable, which will connect Denmark with Netherlands is supposed to became a Multi terminal DC connection in the future. Since currently there are only few operating VSC MTDC connections in the world and none of them located in Europe, the studies regarding MTDC connections are necessary. Since there are few possible control strategies which may be implemented into the MTDC terminals, it is crucial to determine which one is the most reliable in terms of robustness and operability. This project focus is to find this strategy, based on several test and observation of system behaviour. The model and analyses were created and performed in DIgSILENT Power Factory.

## Table of contents

# Nomenclature and Abbreviations

Both Nomenclature and Abbreviations are sorted alphabetically.

## Nomenclature

| Symbol | Unit | Definition |
|---|---|---|
| $\hat{V}_{carrier}$ | kV | Voltage of carrier signal, averaged over one switching period |
| $\hat{V}_{modulated}$ | kV | Voltage of modulated signal, averaged over one switching period |
| $\hat{\lambda}_{abc}$ | kV or kA | Space phasor calculated in $abc$ reference frame (complex number) |
| $\hat{\lambda}_{dq0}$ | kV or kA | Space phasor calculated in $dq0$ reference frame (complex number) |
| $\hat{\lambda}_{\alpha\beta}$ | kV or kA | Space phasor calculated in $\alpha\beta$ reference frame (complex number) |
| $E_{SM}$ | $\frac{kJ}{MVA}$ | Energy that should be stored in a single submodule per MVA |
| $I_c$ | kA | Cable current |
| $K_i$ | depends | Integral gain |
| $K_p$ | depends | Proportional gain |
| $N_a$ | - | Number of sub-modules per arm |
| $P_{tr}$ | MW | Transmitted Power (LCC) |
| $T_i$ | depends | Integral time constant |
| $V_m$ | kV | Peak line-ground phase voltage (LCC) |
| $f_1$ | Hz | Fundamental frequency of output signal |
| $f_s$ | Hz | Frequency of a carrier signal |
| $k_{DC}$ | $\frac{1}{A}$ | Droop Constant |
| $m_a$ | - | Amplitude Modulation Ration |
| $m_f$ | - | Frequency Modulation Ratio |
| $v_c$ | kV | Voltage across submodule |
| $\lambda_a$ | kV or kA | RMS Voltage or RMS Current of phase a |
| $\lambda_{peak}$ | kV or kA | Peak Voltage or Peak Current |
| C | mF | Capacitance |
| f | Hz | Frequency |
| L | mH | Inductance |

| | | |
|---|---|---|
| P | kW | Transferred Active Power (VSC) |
| Q | kVar | Transferred Reactive Power (VSC) |
| $r_{on}$ | Ω | Resistance of a diode or a transistor in a conducting state |
| S | MVA | Apparent Power |
| T | s | Period |
| t | S | time |
| $V_{AC}$ | kV | AC Voltage, RMS Line-Line value |
| $V_d$ | V | On-state Voltage drop |
| $V_{DC}$ | kV | DC Voltage between 2 DC poles |
| $V_s$ | kV | Grid Voltage, RMS Line-Line value |
| $V_t$ | kV | Converter AC terminal voltage, RMS Line-Line value |
| α | o | Firing angle (LCC) |
| δ | o | Angle between $V_s$ and $V_t$ |
| ΔV | kV | Difference in magnitude of $V_s$ and magnitude of $V_t$ |
| ω | rad | Angular Frequency |
| $\varphi$ | rad | Initial phase angle |

# Abbreviations

| Acronym | Definition |
|---|---|
| AC | Alternating Current |
| COBRAcable | **CO**penhagen **BR**ussel **A**msterdam cable |
| CSC | Current Source Converters |
| DC | Direct Current |
| DSL | DIgSILENT Simulation Language |
| EU | European Union |
| HVDC | High Voltage Direct Current |
| IGBT | Isolated Gate Bipolar Transistor |
| Im | Imaginary |
| LCC | Line Commutated Converters |
| MMC | Modular Multi-level Converter |
| MoU | Memorandum of Understanding |
| MTDC | Multi-Terminal Direct Current |

| | |
|---|---|
| MV-MTDC | Multi-Vendor Multi-Terminal Direct Current |
| NSCOGI | North Seas' Countries Offshore Grid Initiative |
| OHL | Over Head Line |
| PCC | Point of Common Coupling |
| PtP | Point-to-Point |
| Re | Real |
| RMS | Root Mean Square |
| SC | Short Circuit |
| SM | Sub-module |
| THD | Total Harmonics Distortion |
| TSO | Transmission System Operator |
| VSC | Voltage Source Converter |
| VSC | Voltage Source Converters |

# List of Figures

# List of Tables

# 1. Introduction

In 2008, the Commission of the European Communities has presented "An EU Energy Security and Solidarity Action Plan" which contained 5 steps suggested to ensure the security of energy supply in all EU member countries, decrease the greenhouse gasses emission and reduce the energy import from outside the EU [**1**]. The first step of this plan is the construction of "the European super grid" which consists of present day power grid and 6 crucial infrastructures [**1**]. One of these structures is the "North Sea Offshore Grid" [**1**]. Since the number of offshore wind farms is increasing, as shown in Figure 1.1 [**2**], and many of those installations are either constructed or planned to be constructed in the north sea [**3**], the "North Sea Offshore Grid" is supposed to be a High Voltage Direct Current (HVDC) grid that would interconnect all countries located on north sea coast and most offshore wind farms.

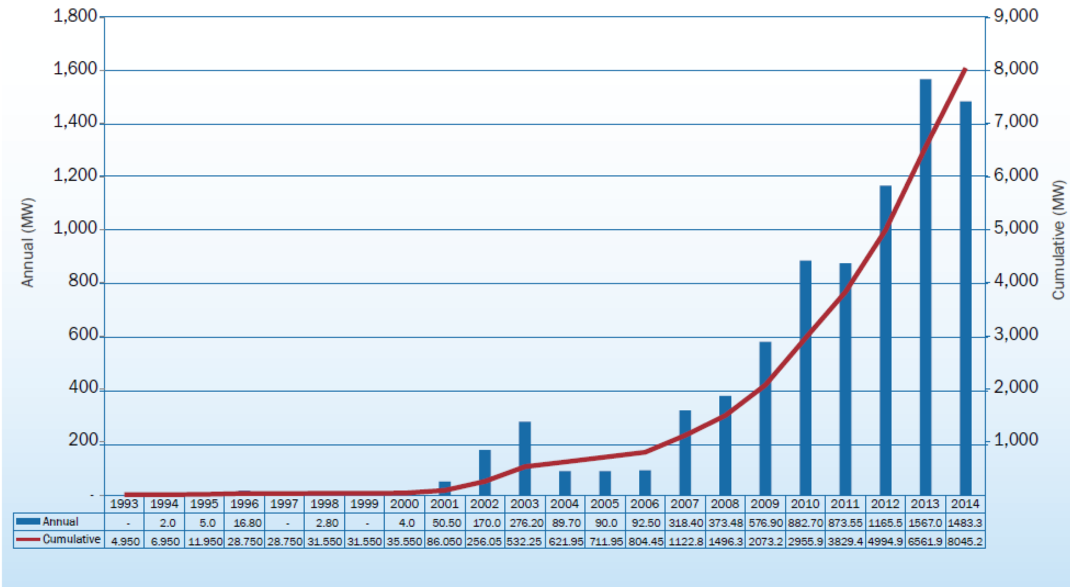


**Figure 1.1 Cumulative and annual offshore wind installations (MW) [2]**

## 1.1 North Seas' Countries Offshore Grid Initiative

To ensure that construction of the "North Sea offshore grid" will not cause a violation of national interests of any involved EU member country, the international coordination is necessary. In December 2009, nine EU member countries (Belgium, Denmark, France, Germany, Ireland, Luxembourg, the Netherlands, Sweden and UK) have signed up a political declaration on the North Seas' Countries Offshore Grid Initiative (NSCOGI) [**4**], which was also signed by Norway in January

2010 [5]. NSCOGI is a cooperation program between 10 previously mentioned countries, which was formalised by signing a Memorandum of Understanding (MoU) in 2010 [6]. The program is supported by governments and regulators and Transmission System Operators (TSOs) of every country which signed the MoU, as well as the European Commission [6].

In 2011 one of 3 working groups in NSCOGI has presented the report regarding the forecasted grid design changes over time [7]. The visual representation of assumed grid changes is presented in Figure 1.2 [7]. The present radial coordination will be changed to local coordination, then to international coordination, to finally become the meshed solution. In radial solution, all HVDC connections are realized as Point-to-Point (PtP) connections, which means that there are only 2 terminals in one connection. However, in 3 other solutions several windfarms are connected with each other and with one or more points onshore through a DC connection, which means that there are more than 2 terminals in those connections. This type of connection is known as Multi-terminal DC (MTDC) connection [8]. If in one MTDC connection there are terminals from at least 2 vendors (manufacturers), this type of MTDC is known as Multi-Vendor MTDC (MV-MTDC) [8].

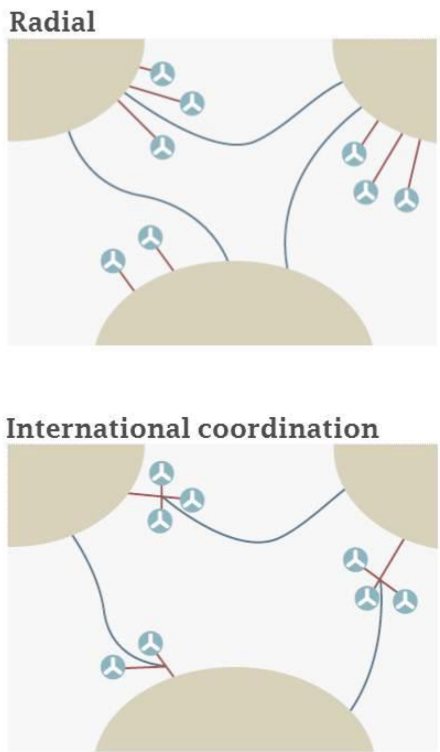


Figure 1.2 Assumed General Pattern of Offshore Grid Development [7]

## 1.2 COBRAcable

In 2010 a new interconnection project has been initialized by two European TSOs, Energinet.dk from Denmark and TenneT from Netherlands [**9**]. The project has received a name "COBRAcable" (Acronym of **CO**penhagen **BR**ussel **A**msterdam) and was approved by both TSOs in 2013 [**10**]. Figure 1.3 depicts the HVDC submarine cable connection between Endrup in Denmark and Eemshaven in the Netherlands which is expected be finished in 2019 [**10**].

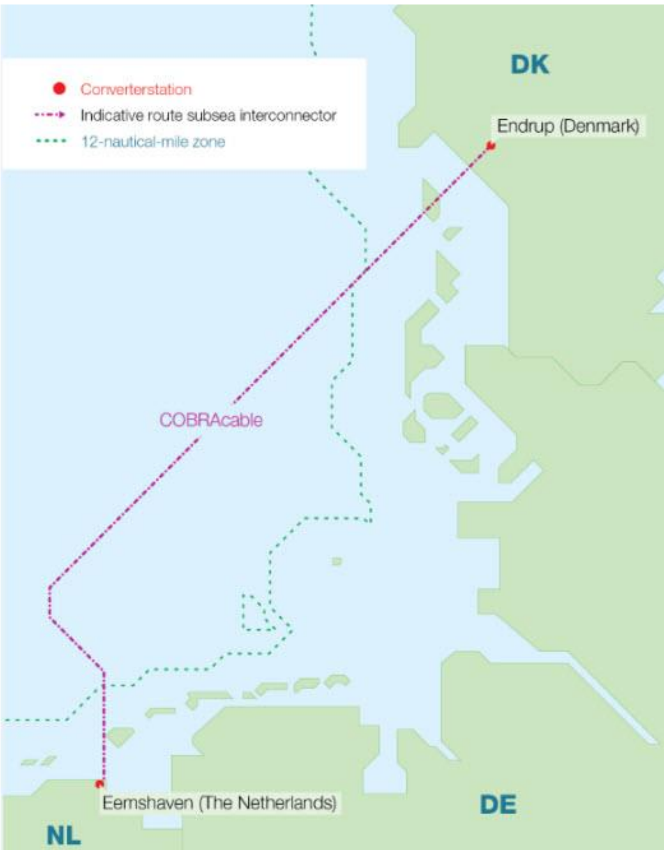


**Figure 1.3 COBRAcable planned route** [10]

The known parameters of COBRAcable [**10**]:

- Length – 350 km
- Nominal Voltage – ±320 kV
- Rated Power – 700 MW
- Technology – Voltage Source Converter (VSC)

The COBRAcable may become an MV-MTDC connection in the future, thus becoming a part of the "North Sea offshore grid" [**10**]. Therefore, it should be determined what control strategy should be implemented in COBRAcable terminals in the future.

## 1.3 Problem Statement and Objectives

Since COBRAcable is supposed to be expanded into an MV-MTDC connection, a proper control strategy needs to be implemented to ensure the operability, robustness and reliability of the HVDC system. The main goal of this project is to determine what control strategy should be implemented in terminals of an expanded COBRAcable.

In order to obtain the necessary solution, the following objectives must be achieved.

- Create generic models of both PtP and MTDC connections in DIgSILENT PowerFactory.
- Create control models for both connection type models.
- Test control modes models on PtP model and tune PI controllers for maximum effectiveness.
- Investigate the behaviour of the MTDC model with different control strategies under following events:
    - 3 phase short circuit
    - Reduced power transfer
    - Loss of converter
- Investigate the sensitivity of the system based with regards to changes in following factors:
    - Outer controller type and values
    - Inner controller type and values
    - Droop constant values
- Use obtained data to determine which strategy shows the best performance in terms of operability

## 1.4 Limitations

The following limitations have been included in the project:

- MTDC connection model consists of 3 terminals, 2 onshore substations and one offshore wind farm
- Only the unconcealed data regarding COBRAcable connection are implemented.
- The control of Reactive power is skipped due to MTDC's main focus on active power and DC voltage control
- The control mode implemented into the VSC terminal can't be changed during the simulation
- The reference AC voltage and frequency of offshore wind farm are both constant parameters

## 1.5 Report structure

In the second chapter, the state of the art of HVDC connections is presented, with a brief history and advantages of power transfer by a DC in the beginning. Then, currently used converter topologi es are presented, where MTDC topology is described with more details. Afterwards two converter technologies are presented and described, Line Commutated Converters (LCCs) and Voltage Source Converters (VSCs). The description of LCC includes the description of electric components installed in its substation, the configurations in which it may operate, the current conversion process explained on the ideal converter which operates in basic configuration and the basic operation principle. The VSC description is constructed in a same way, however since this technology is used in the COBRAcable, all sections are described with more details and there is additional section which presents a non-ideal converter. At the end of the chapter, the converter technologies are compared with each other.

Chapter 3 presents concepts and methods to control HVDC connections. At the beginning, the ideas of control hierarchy and levels of control are presented. Then, the transformations between reference frames and space phasor are presented, since it is essential mathematical tool in an HVDC control. The upper level control strategies and modes are then presented, in order to determine which of them should be implemented in the model. After the upper level controls determination the dispatch control strategies are presented for both PtP and MTDC connections. The determination of MTDC dispatch controls that will be implemented in the model concludes this chapter.

Fourth chapter presents the generic models of PtP connection, MTDC connection and control modes, which were created in DIgSILENT Power Factory.

Chapter 5 was supposed to present the description of tests performed on each model, along with implemented inconstant data and obtained results. Based on those results, the best strategy for MTDC connection was supposed to be determined. Due to run out of time, only the description of planned tests is included.

Final chapter presents the conclusions obtained in this project along with suggested future work and possible improvements.

# 2. HVDC Transmission Systems

High-voltage direct current (HVDC) is a power transmission system in which the current is converted from AC to DC and power is transported via a DC cable or overhead line (OHL) [**11**]. A simple idea schematic is depicted in Figure 2.1.

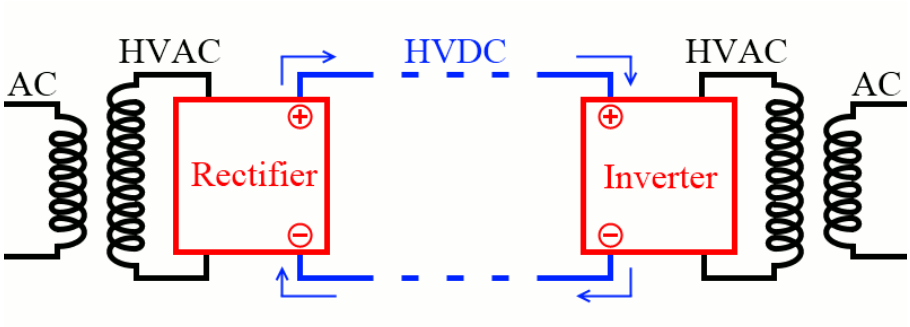


**Figure 2.1 Idea schematic of an HVDC connection** [12]

The first HVDC connection was created in 1950s in Europe. With improving technology of converters, more HVDC connections were built all around the world. Currently there are over 170 existing HVDC connections [**13**]. Figure 2.2 depicts some of them.

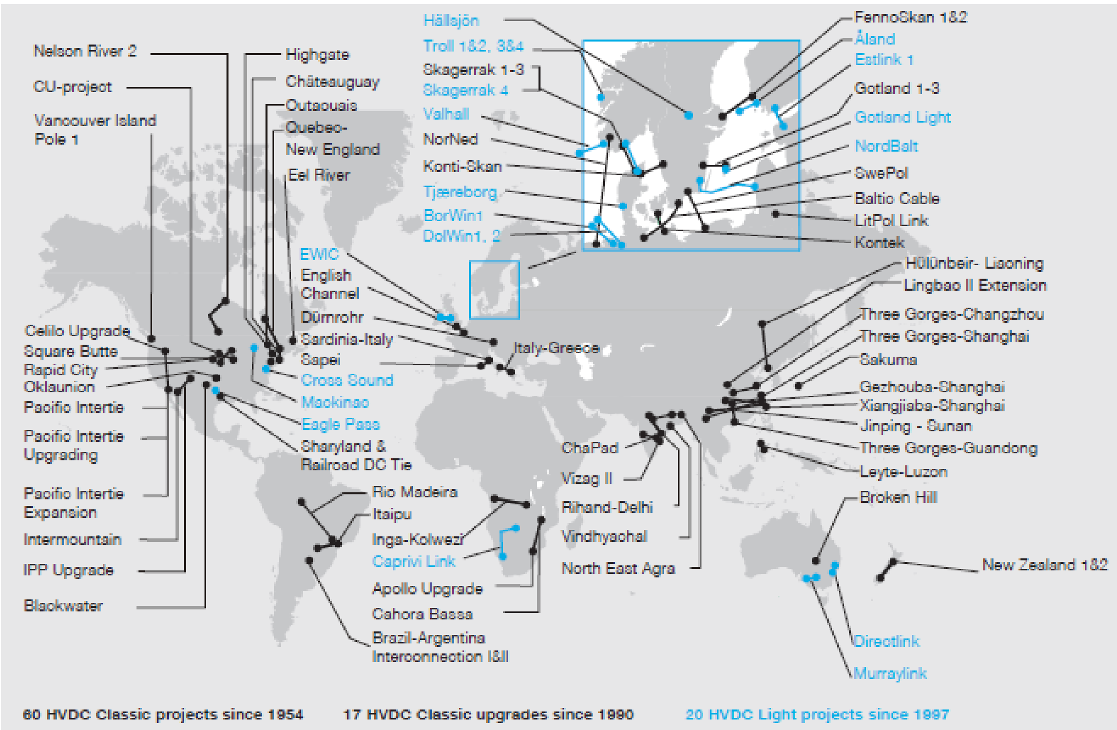


**Figure 2.2 Some of currently existing HVDC connections** [14]

## 2.1 Advantages of HVDC

DC transmission systems have numerous technical, economic and environmental advantages over AC transmission systems:

- **Asynchronous grids connection** – Many electrical grids are asynchronous to each other. This is caused by either different nominal frequency or different phasor angle at the same time e.g. continental Europe grid and Nordic grid are asynchronous, even though nominal frequency for both of them is 50 Hz. In this case, connecting them via AC line is impossible, however DC line is a good solution, since converters on each end of HVDC line will work with respect to their AC side grid parameters [**14**].
- **Power control** – In AC system, active and reactive power flow depends on power demand, while reactive power depends also on shunt reactors. With HVDC converters, it is possible to directly control active power flow (with LCC and VSC) and reactive power flow (only with VSC) [**15**].
- **Low short circuit current** – HDVC transmission line does not rise the SC current level. [**14**]. Due to this feature, it might be good solution for some big cities, which SC current level is currently close to its maximum limit e.g. Copenhagen [**16**]
- **Lower power losses and investment cost on long distances** – The HVDC connection terminals causes higher power losses than AC terminals while being more expensive. Thus for short distances the AC transmission is more cost effective. However, the capacitance of AC lines and cables causes high power losses on long distances, due to generation of reactive power that needs to be compensated. On the other hand, the capacitance of DC lines and cables doesn't cause the reactive power generation, therefore for submarine cables longer than 80 km [**17**] and OHL longer than 600-800 km [**17**] an HVDC becomes more feasible solution. This is depicted in Figure 2.3. [**14**] and Figure 2.4 [**14**]

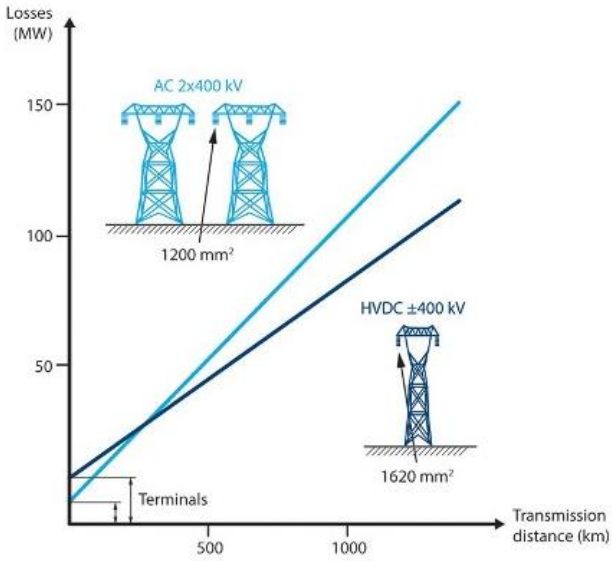


**Figure 2.3 Power losses in transmission lines [14]**

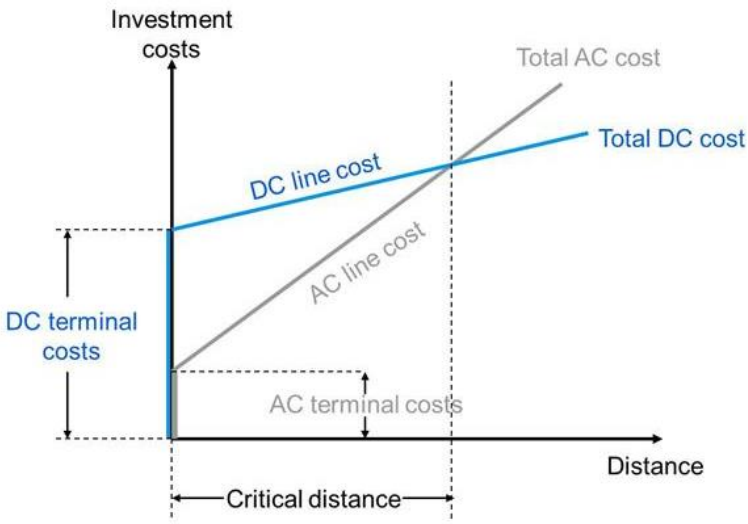


**Figure 2.4 Cost of transmission lines [14]**

## 2.2 Converter Topologies

The common HVDC topologies are presented graphically from Figure 2.5 to Figure 2.9, with brief description of each of them.

### 2.2.1 Asymmetric Monopole

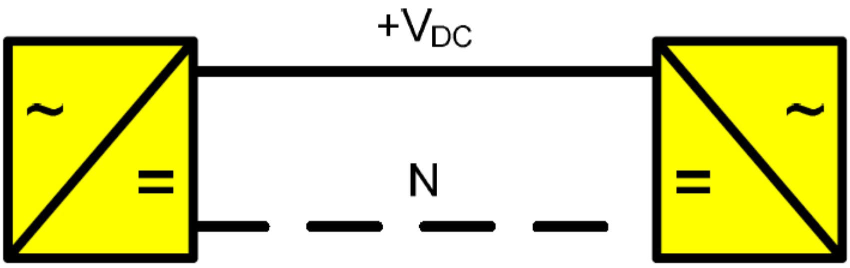


Figure 2.5 Asymmetric monopole [18]

The basic HVDC configuration. It consists of one converter on each side of DC OHL or cable. The return path is either through metallic connection or ground. The name of this configuration comes from fact, that the line-ground voltage in point N is equal to 0, while line-ground voltage in point $+V_{DC}$ is equal to the rated voltage of DC line.

### 2.2.2 Symmetric Monopole

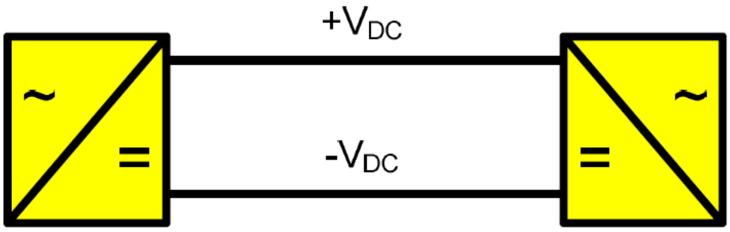


Figure 2.6 Symmetric Monopole [19]

In this monopole variation, there are 2 HVDC transmission lines, one with positive and one with negative line-ground voltage. This topology can't be applied with LCC technology, since a 6-pulse converter works as asymmetric monopole, while higher pulse bridges are treated as bipoles.

### 2.2.3 Bipole

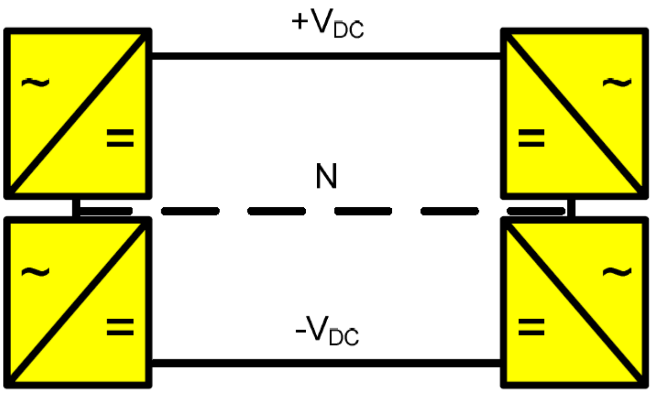


Figure 2.7 Bipole [19]

This topology consists of 2 converters on each terminal. The transmission capacity in bipole is higher than in monopole, which rises the amount of power which can be transferred. In case when one pole is under maintenance, it is possible to use the other pole, thus Bipole is more reliable for security of supply [**20**].

### 2.2.4 Back-to-Back

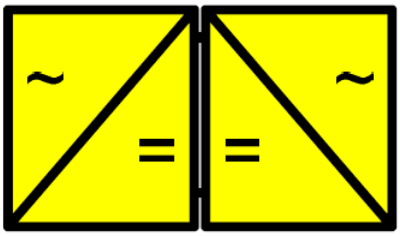


Figure 2.8 Back-to-Back

This topology doesn't have an OHL or DC cable between converters, because they located in the same building. This is common solution for connection of 2 unsynchronized AC grids, that are close to each other.

### 2.2.5 Multi-Terminal DC

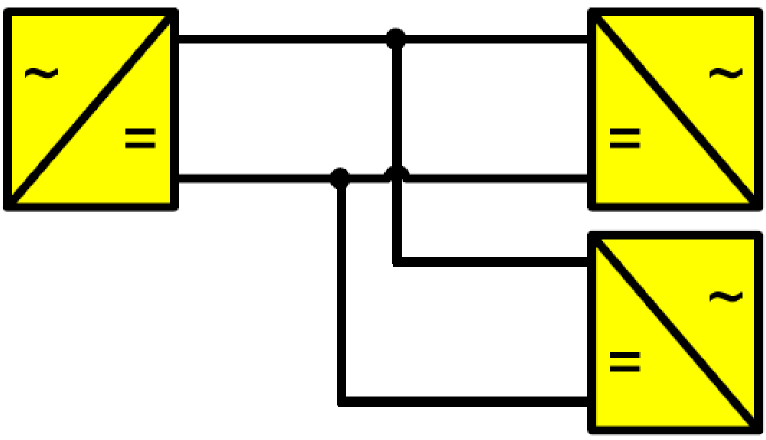


Figure 2.9 MTDC [18]

MTDC is an HVDC connection between more than 2 terminals. The idea of a parallel MTDC connection, shown in Figure 2.10 (b), was presented in 1963 [**21**], followed by a series connection, shown in Figure 2.10 (a), presented 2 years later [**21**].

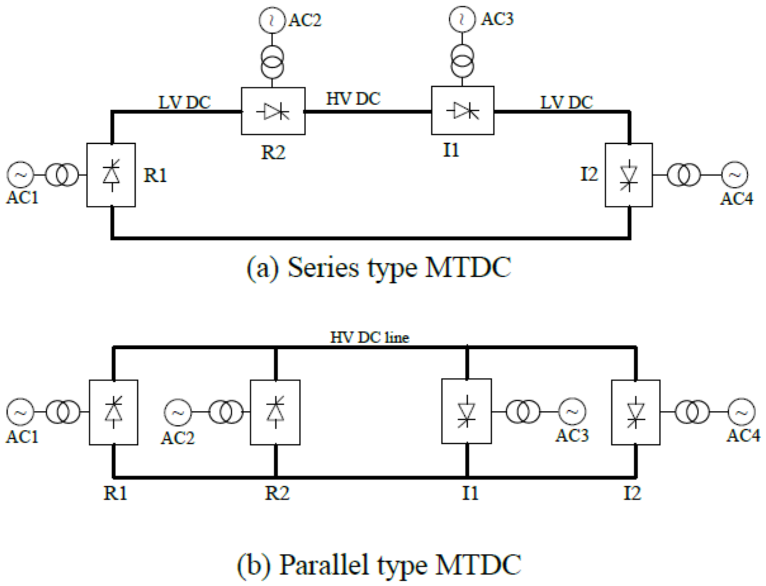


Figure 2.10 LCC MTDC solutions: series (a) and parallel (b) [21]

In 2011, there were 2 MTDC LCC connections operating and 3[rd] connection in development [**22**]. Such small number of LCC-MTDC connections is caused by a fact that in order to change the direction of power flow in LCC-HVDC, the voltage polarization needs to be changed. Moreover, if a short circuit occurs in a cable between $R_2$ and $I_1$ in Figure 2.10(b), the thyristors at both of those points need to be rotated by $180^{O}$ in order to keep the rest of the DC grid operating. This is the reason why in existing LCC-MTDC connections the power flow is fixed [**22**].

The VSC-MTDC connections also can be built as series connection, which is known as ring topology and is presented in Figure 2.11, or star topology, presented in Figure 2.12. The voltage polarization doesn't need to be changed in VSC and the power flow direction can be easily switched by changing the current flow. Because of this MTDC projects with unfixed power flow, such as COBRAcable, are developed with VSC technology. Currently there are only few operating VSC-MTDC connections in China [**23**].

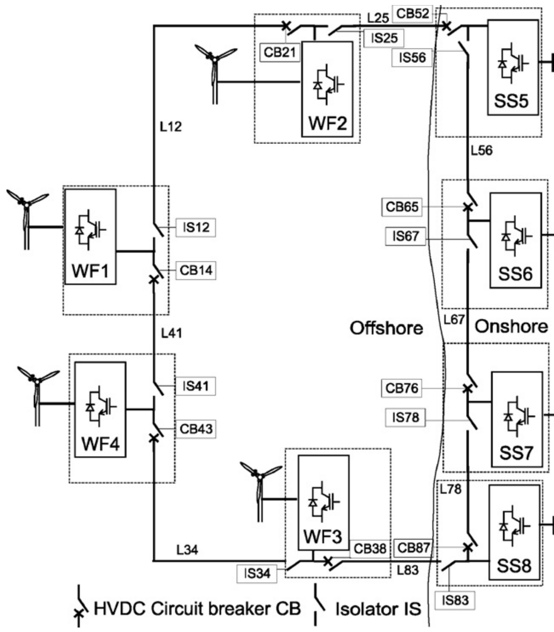


Figure 2.11 Ring topology [24]

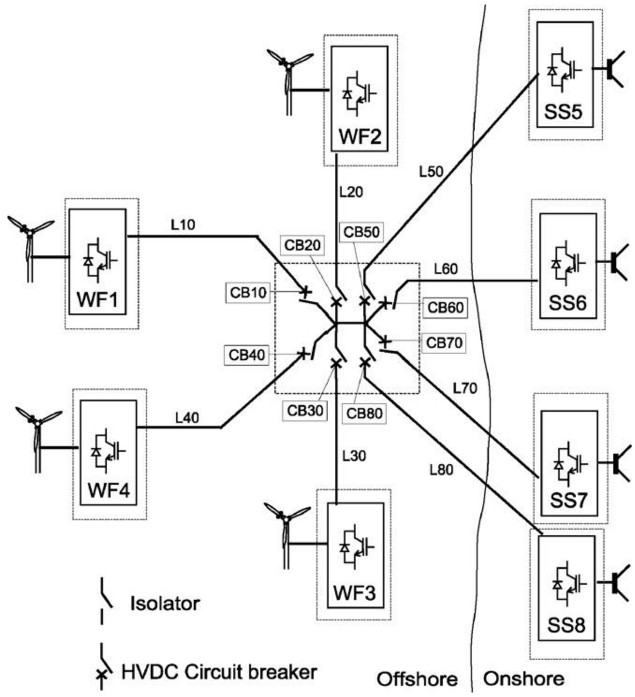


Figure 2.12 Star topology [24]

## 2.3 Line Commutated Converters

Line Commutated Converter (LCC) also known as Current Source Converter (CSC) is a converter technology in which thyristor valves are used for current conversion [**25**]. This technology was first used in 1967, when one of mercury arc valves in Gotland 1 connection was replaced with thyristor valve. Currently, it is considered the most economical way to transfer huge amount of power, up to 8000 MW, over very long distances [**14**].

### 2.3.1 LCC Components

Figure 2.13 depicts a simplified LCC- HVDC converter station schematic. Description of station components is presented below the figure.

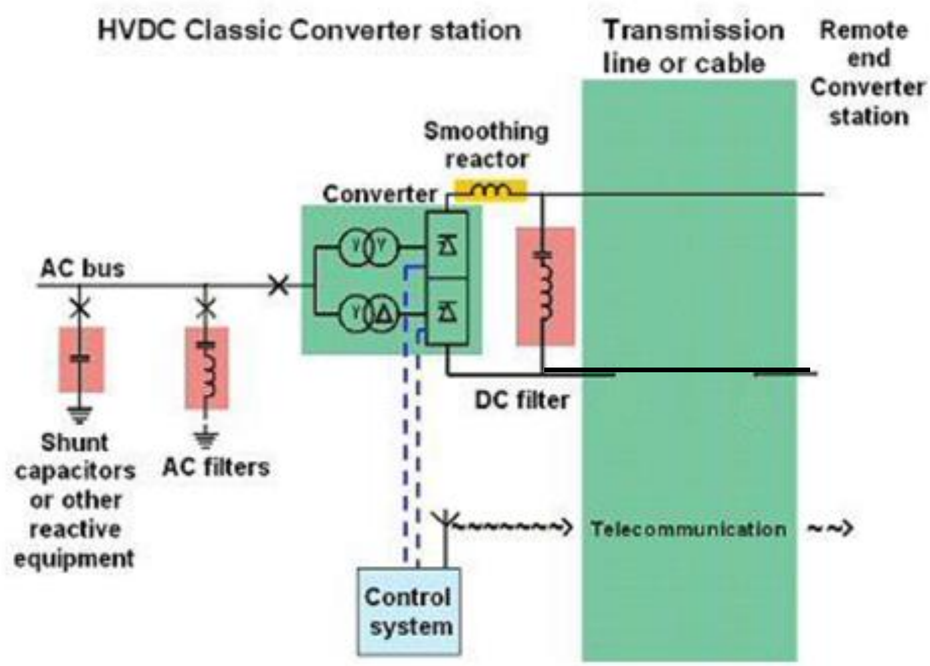


Figure 2.13 LCC-HVDC converter station [22]

- **Converter** – This element consists of transformers connected in series with thyristor valves. Each rectangle with thyristor symbol inside represent a six-pulse bridge converter.
- **Transmission line** – a DC OHL or cable. It exists in every topology except back to back.
- **AC filters** – Device responsible for blocking high current harmonics, generated by converters, from penetrating the AC grid.
- **DC filters** – Device that smoothes the ripples of DC voltage.
- **Shunt capacitors** – Source of reactive power, required to maintain the voltage on AC busbar.
- **Control System** – A system that transmits control signal to thyristors.

### 2.3.2 Current Conversion in ideal LCC-HVDC

The AC/DC conversion with LCC technology is explained on the six-pulse bridge example, depicted in Figure 2.14. For simplicity of explanation, the following assumptions are made:

- Firing angel $\alpha=0^{O}$ (control signal explained with more details in section 2.3.3), thus thyristors behave like diodes
- Thyristors are treated like short circuit while being forward biased (conducting state)
- Thyristors are treated as open circuit while being reversed biased (blocking state)
- Transitions from blocking state to conducting state and vice versa are instant
- There is no commutation overlap

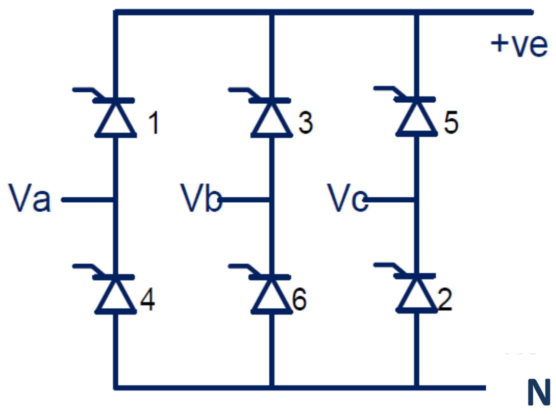


**Figure 2.14 Six-pulse bridge** [26]

Voltage waveforms of 6-pulse bridge converter that converts AC to DC are depicted in Figure 2.15. The top chart shows line-ground AC voltages of 3 phases over one period. When thyristors 1 and 2 are in conducting state and the rest is in blocking state, the line-ground voltage at point +ve is the same as line-ground voltage of phase A, while voltage at point N is equal to line to ground voltage of phase C. At one point, line-ground voltage of phase B will become higher than voltage of phase A, thus the thyristor nr 3 will switch into conducting state. At the same moment, thyristor nr 1 will become reversed biased, thus switching into blocking state. Similar change of states will occur in thyristors 2 and 4, with difference that the voltage of phase A will become lower than voltage of phase C. Voltage changes will cause further simultaneous switching in thyristors 3 and 5, 4 and 6, 5 and 1, 6 and 2 over one period. This causes the line-ground voltage at point +ve to be always the same as the highest positive phase voltage, which is depicted in medium chart as blue line. Consequently, the line-ground voltage at point N is always the same as highest negative phase voltage, which is depicted in medium chart as red line. The bottom chart shows an output DC voltage between +ve and N. There are 6 pulses on DC voltage over one AC voltage period, thus the name 6-pulse bridge.

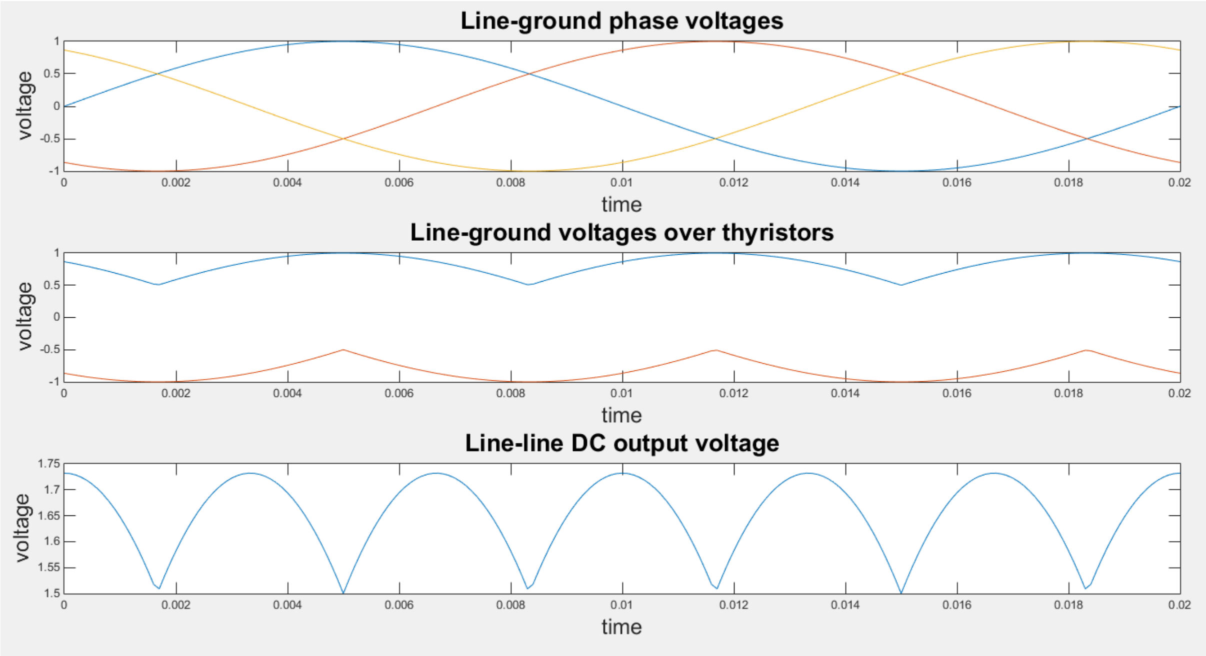


Figure 2.15 Voltage waveforms in 6-pulse bridge converter

### 2.3.3 Basic Operation of ideal LCC-HVDC

Thyristors receive one control signal, the firing angle α. This angle corresponds to time that thyristor have to wait before start conducting the signal. With $\alpha=0^{0}$ thyristors behave like diodes and the power is conducted as soon as thyristors became forward biased. Thyristors will stop conducting when current that flows through them will reach 0 A. The waveforms of output DC voltage in this case looks similar as in bottom graphs of Figure 2.15 and Figure 2.17. The active power flow is regulated by adjusting the firing angle α. If $0^{0}\leq\alpha<90^{0}$, the converter works as a rectifier, which means that power flow goes from AC grid to DC transmission line. If $90^{0}<\alpha\leq180^{0}$ the converter works as an inverter and the power flow goes from DC transmission line to AC grid. Those margins are genuine only for ideal LCC converter, in real converters issues like commutation overlap (time when 3 thyristors commutates at the same time) and risk of commutation failure results in more narrow margins. Assuming no commutation overlap and converter power losses, the amount of power transmitted by converter is described by Equation 2.1 [**26**].

$$P_{tr} = \frac{3\sqrt{3}}{\pi} V_m \cos(\alpha) I_c \qquad 2.1$$

Where:

$P_{tr}$- Transmitted power

$V_m$- Peak line-ground phase voltage

$I_c$- Cable current

### 2.3.4 LCC Configurations

In Figure 2.13 there are 2 six-pulse bridges connected in series, which creates a 12-pulse bridge. More detailed picture of 12-pulse bridge converter is depicted in Figure 2.16.

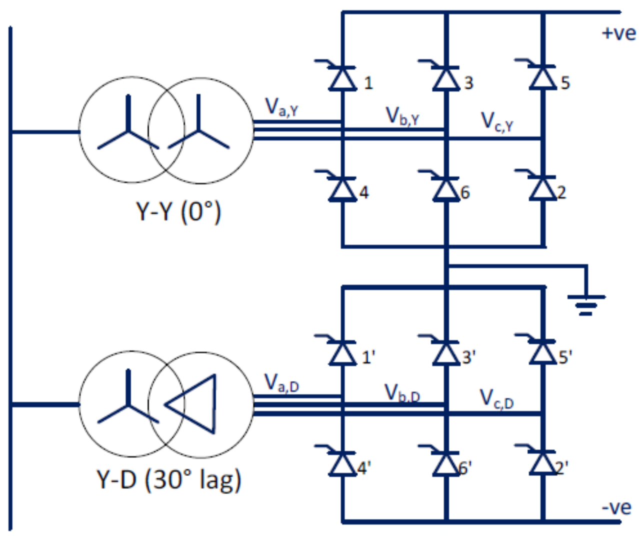


**Figure 2.16 Twelve-pulse bridge converter** [26]

The winding configuration of 2nd transformer is crucial in 12-pulse bridge converter operation. By using Y-Δ winding configuration in 2nd transformer a phase shift of 30$^{O}$ is created between phase voltages in upper bridge and lower bridge. The construction of both bridges is the same, therefore the DC voltage over lower bridge will have the same shape as corresponding voltage over upper bridge but with 30$^{O}$ lag, which is depicted in the top chart in Figure 2.17. Blue line shows the voltage over 6-pulse bridge connected to Y-Y transformer, that is voltage between +ve line and ground. Red line depicts voltage over 6-pulse bridge connected to Y-delta transformer, that is voltage between ground and –ve line. The output voltage of 12-pulse bridge is a sum of 2 voltages shown in top chart, which is depicted in the bottom chart.

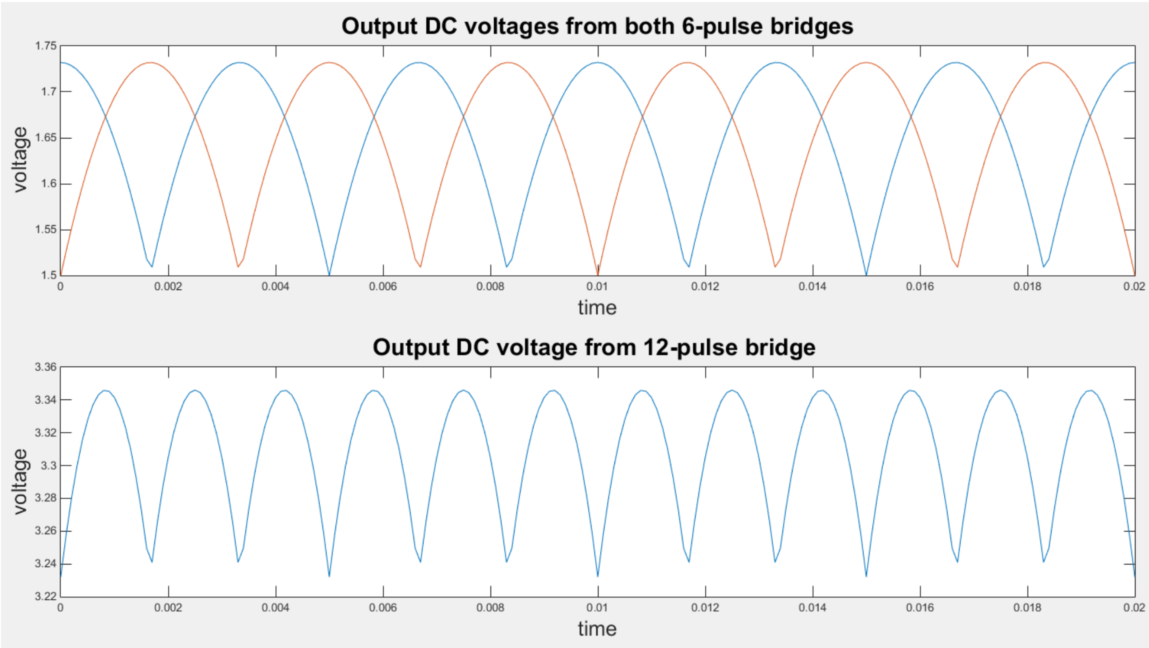


**Figure 2.17 Voltage waveforms in 12-pulse bridge converter**

The ripples in 12-pulse bridge is smaller than in 6-pulse bridge, which means that the total harmonics distortion (THD) have been reduced. This is confirmed in Table 2.1 [**27**].

**Table 2.1 Typical values of current harmonics for different types of front ends [27]**

| | Harmonic order ($h$) | 5 | 7 | 11 | 13 | 17 | 19 | 23 | 25 | $THD_i$ |
|---|---|---|---|---|---|---|---|---|---|---|
| Typical values of harmonic current (% of fundamental current) of different types of front end configurations (% $I_h/I_1$) | 6-pulse without line reactor (Stiff source) | 80.0% | 58.0% | 18.0% | 10.0% | 7.0% | 6.0% | 5.0% | 2.5% | 101.5% |
| | 6-pulse with 2-3% line reactor | 40.0% | 15.0% | 5.0% | 4.0% | 4.0% | 3.0% | 2.0% | 2.0% | 43.6% |
| | 6-pulse with 5% line reactor | 32.0% | 9.0% | 4.0% | 3.0% | 3.0% | 2.0% | 1.5% | 1.0% | 33.9% |
| | 6-pulse with line harmonic filter (LHF) | 2.5% | 2.5% | 2.0% | 2.0% | 1.5% | 1.0% | 0.5% | 0.5% | 4.9% |
| | 12-pulse | 3.7% | 1.2% | 6.9% | 3.2% | 0.3% | 0.2% | 1.4% | 1.3% | 8.8% |
| | 18-pulse | 0.6% | 0.8% | 0.5% | 0.4% | 3.0% | 2.2% | 0.5% | 0.3% | 3.9% |

The 5th and 7th harmonics are significantly reduced in 12-pulse bridge and are no longer dominant. For 18 and 24-pulse bridge, the harmonics can be further reduced, yet it requires additional transformers with particular winding configuration. Those configurations and the change of phase angle they create is depicted in Figure 2.18.

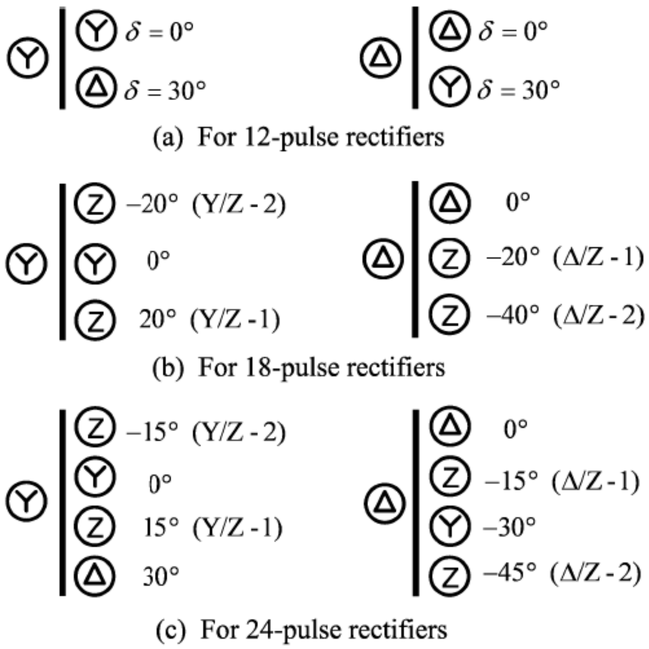


Figure 2.18 Transformer winding configurations and obtained phase angle change [26]

## 2.4 Voltage Source Converters

Voltage Source Converter (VSC) technology was introduced in 1997 by ABB. In this technology, the thyristors have been replaced by IGBTs. The maximum power capability of IGBTs is lower than thyristors, as shown in Figure 2.19 [**28**] .

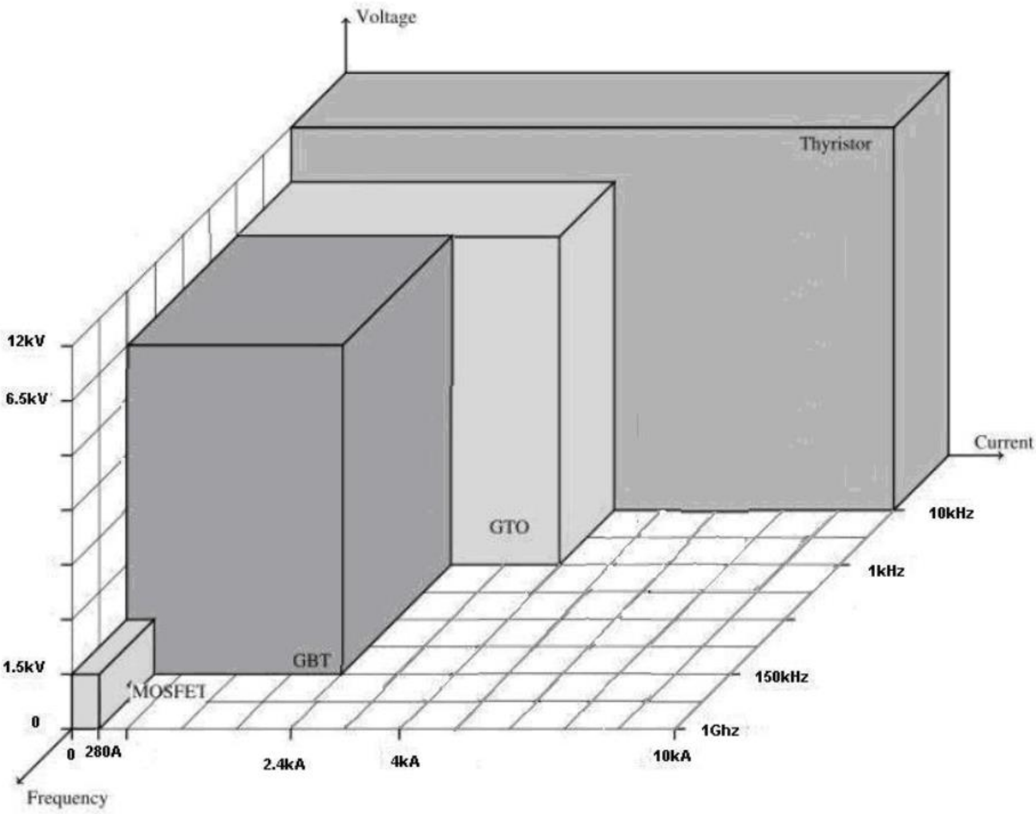


Figure 2.19 Ratings of power semiconductor devices [28]

On the other hand, VSC allows usage of HVDC in more applications than LCC e.g. wind power connection or power transfer to oil platforms [**14**]. One of reasons for its wider application usage is the fact, that LCC converter requires strong grid to be connected into. The ratio of SC power to nominal power on converter terminals have to be bigger than 2 for LCC, while VSC converters don't have this restriction, thus can be installed In weak grids and islanded networks [**18**]. Another reason is the size of LCC station, compared to VSC station. While 500 MW LCC station requires approximately 225m x 120m area, VSC station with the same power rating requires only 180m x 115m area [**18**].

### 2.4.1 VSC Components

Figure 2.20 depicts an example of VSC-HVDC connection. Elements in the figure are described below it.

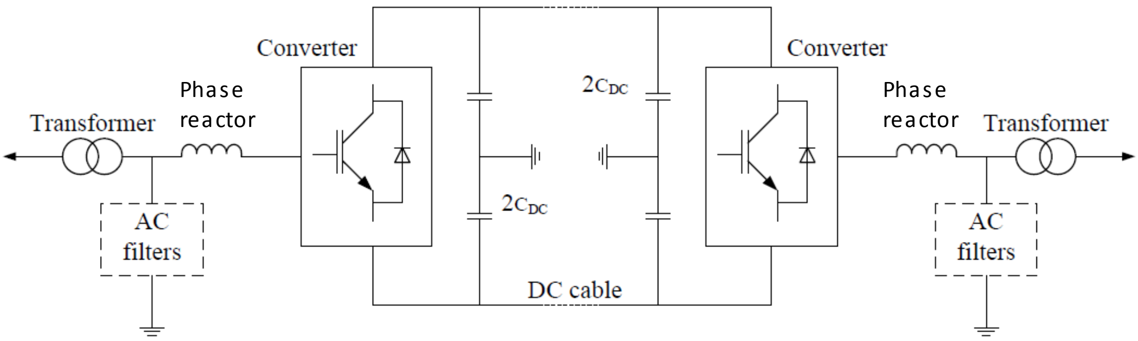


Figure 2.20 Example of a VSC-HVDC connection [29]

- **Converter** - As in LCC, this is the component responsible for AC/DC conversion and vice versa. Thyristor valves have been replaced by IGBTs.
- **DC transmission line** – OHL or cable, which connects 2 VSC-HVDC stations.
- **Transformers** – Equipment which converts the AC voltage to the level suitable for VSC converter. Opposite to LCC, VSC converters doesn't require transformers with particular winding configuration since there is no need for phase shift. In fact, VSC converters need only one transformer, unless the system is supposed to transfer more power than rated power of a single transformer, or to ensure the security of supply in case where one transformer is under maintenance.
- **Phase Reactors** – By regulating current, this component take part in control of active and reactive power. Additionally it works as a low pass filter [**30**]
- **AC filters** – As in LCC, its main purpose is to filter the higher harmonics from the system. However, the VSC contains harmonics of much higher number than LCC, thus the size of those filters in VSC station is greatly reduced, compared to LCC station [**30**]
- **Capacitors** – they reduce the DC voltage ripples, provide a low inductive path for turn off current and store the energy required for power flow [**30**].
- **Control system** – This part is responsible for creating control signal, that will be sent to IGBTs.

### 2.4.2 Current Conversion in ideal VSC-HVDC

The DC/AC conversion is explained on the 2 level VSC configuration, which is depicted in Figure 2.21. For simplicity of example, conversion process is described only for one phase.

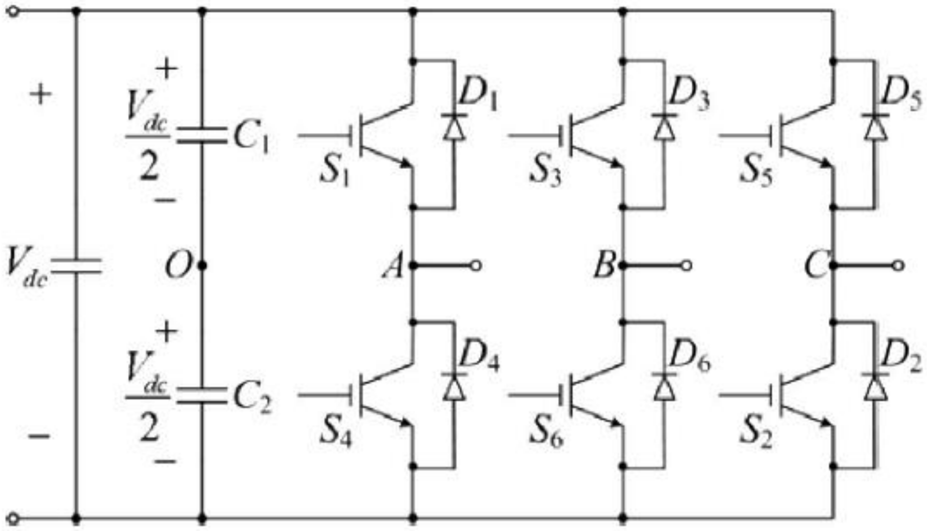


Figure 2.21 Two level VSC topology [31]

To explain the DC/AC conversion in a VSC, a Pulse Width Modulation (PWM) has to be introduced. A mechanism of PWM control for switches 1 and 4 is depicted in Figure 2.22 [**32**]. The control system generates 2 signals, the carrier signal and the modulating signal. The carrier signal is a triangular wave, constant in its magnitude and frequency. The modulating signal have adjustable shape, magnitude and frequency. Control of modulation signal is further described in section 2.4.3. For simplicity of this example, a modulating signal is treated as a sinusoidal signal with constant amplitude and frequency. The carrier and modulating signals are compared with each other. If the carrier signal is smaller than modulating signal, switch $S_1$ is closed and switch $S_4$ is open. When carrier signal becomes bigger, switch $S_1$ gets open and switch $S_4$ is closed. This is depicted in Figure 2.23 [**32**].

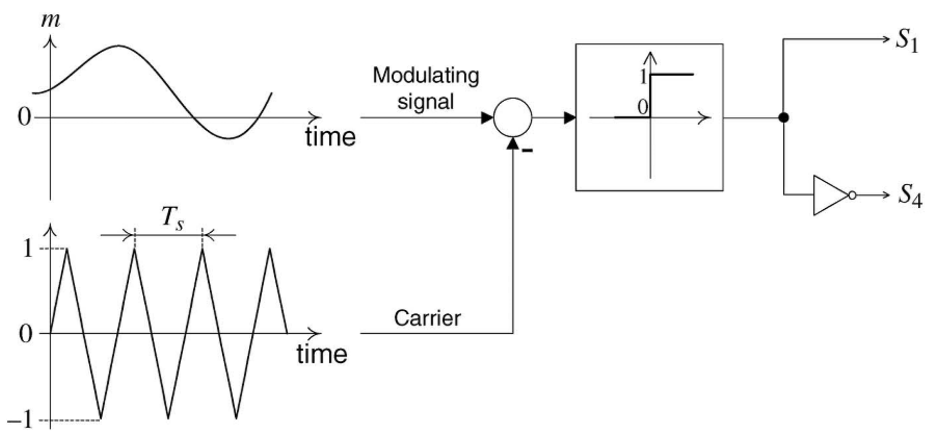


Figure 2.22 Schematic diagram of mechanism used to generate PWM for switches 1 and 4 [32]

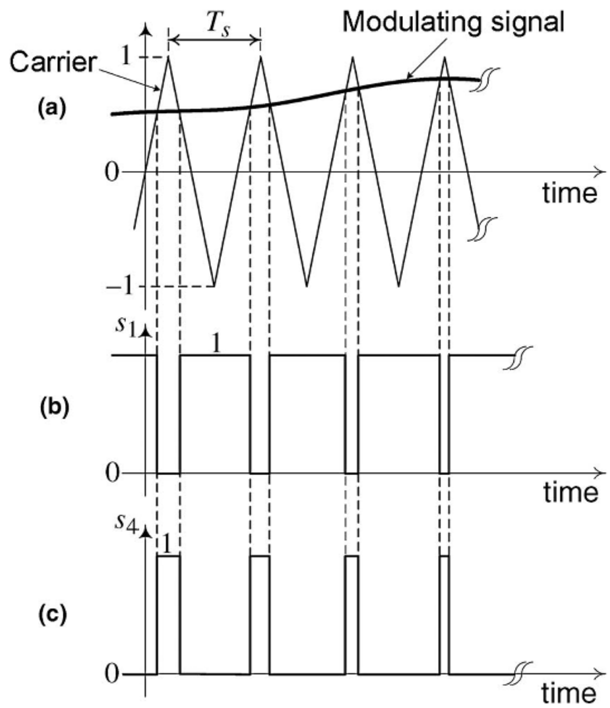


Figure 2.23 Signals based on PWM switching strategy [32]
(a) carrier and modulating signals
(b) switching function of the switch $S_1$
(c) switching function of the switch $S_4$

The carrier signal frequency is much higher than modulating signal frequency, therefore for one period of carrier signal, the modulating signal can be assumed to be a constant DC value. Another assumption is that capacitors $C_1$ and $C_2$ at Figure 2.21 are fully charged. Using these 2 assumptions leads to a simplified power circuit diagram for phase A, depicted in Figure 2.24. To further simplify explanations, additional assumptions are made:

- Transistors and diodes act as a short circuit in conducting state
- Transistors and diodes act as an open circuit In blocking state
- There is no turn-off tailing current in transistors
- There is no turn-off reverse recovery current in diodes
- Switch from conducting to blocking state and vice versa is instant for both diodes and transistors

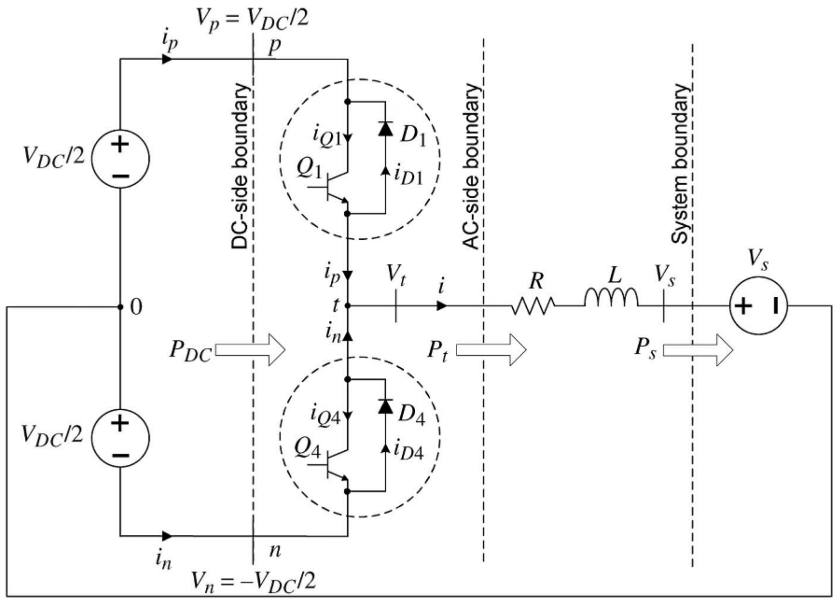


**Figure 2.24 Simplified power circuit diagram [32]**

Voltage source $V_s$ have its plus sign as in Figure 2.24 when phase-ground voltage of phase A is positive. For negative half-wave, polarity of voltage source $V_s$ is reversed. For both of those situations, either switch $Q_1$ or $Q_2$ is opened, which gives 4 possible states of current flow. The waveforms of voltage and current in all 4 states are presented in Figure 2.25. Left side presents voltage waveforms for positive $V_s$ while right side presents waveforms for negative $V_s$. First 2 charts on both sides show the state of both switches, where value 1 means that the switch is closed. The voltages and currents have same indexes as in Figure 2.24.

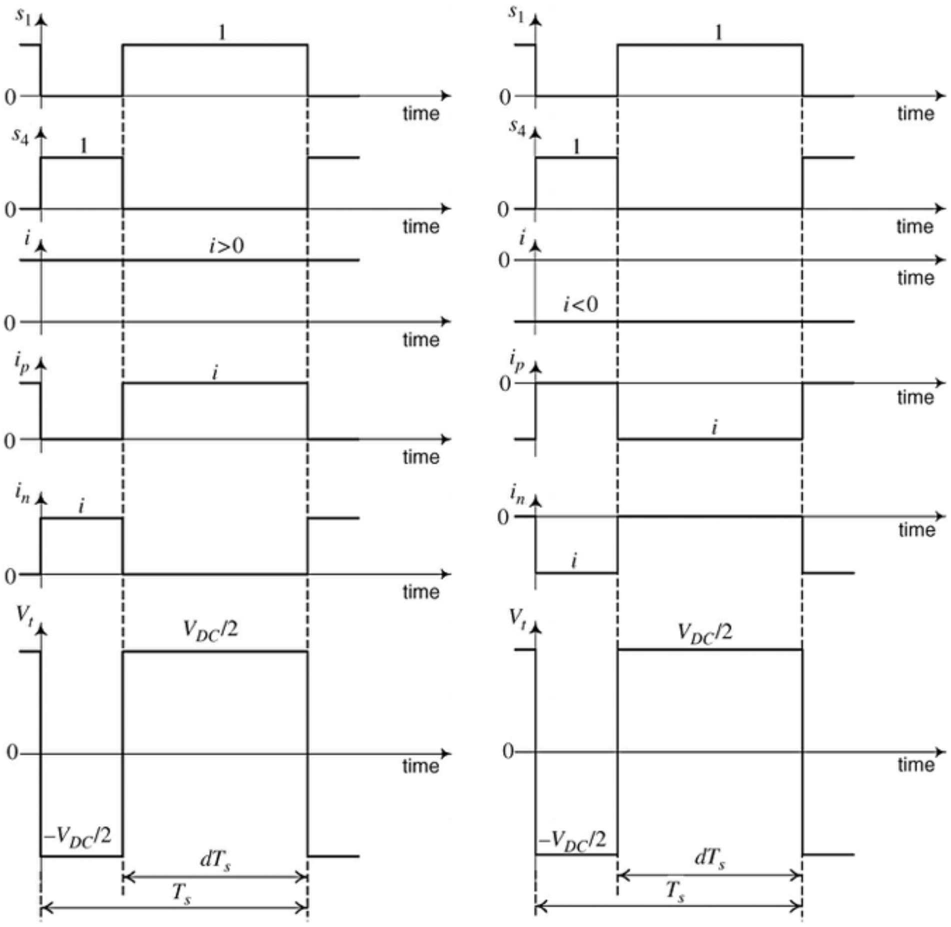


**Figure 2.25 Two level ideal VSC switching model waveforms [32]**
**(left) positive $V_s$**
**(right) negative $V_s$**

The bottom waveforms on both sides shows that the DC voltage has been conversed to the AC voltage. However the output signal is not sinusoid, since AC voltage has value of either $+\frac{V_{DC}}{2}$ or $-\frac{V_{DC}}{2}$. These are the only 2 voltage levels possible to achieve with this configuration, thus the name 2 level VSC. Top chart in Figure 2.26 depicts the voltage waveforms of modulating (here marked as reference) voltage and carrier voltage, while output signal is depicted on the bottom chart. The output signal is not a sinusoid, however its fundamental frequency is the same as voltage frequency in the AC grid. Thus, by applying AC filters that reduce higher harmonics, a sinusoid signal is obtained and the DC/AC conversion is completed.

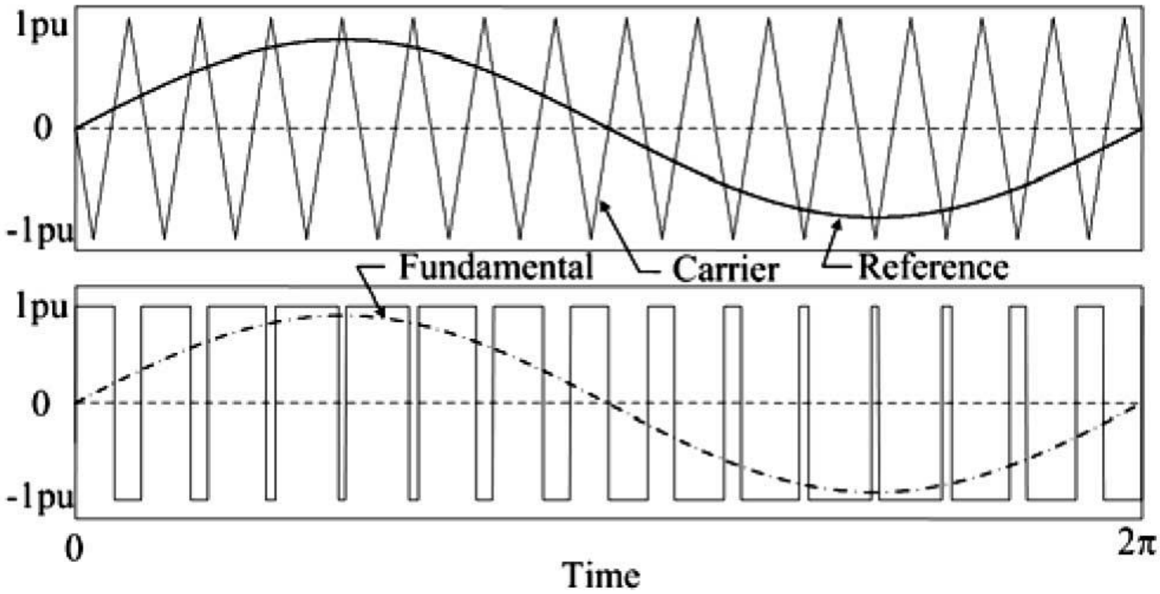


Figure 2.26 Control and output voltage waveforms in 2 level VSC [31]

### 2.4.3 Basic operation of ideal VSC-HVDC

As mentioned in section 2.4.2 the control signal in VSC is modulating signal. The output signal from converter depends on Amplitude modulation ratio ($m_a$) and Frequency modulation ratio ($m_f$), which are described by equations 2.1 and 2.2 [**33**].

$$m_a = \frac{\hat{V}_{modulated}}{\hat{V}_{carrier}} \qquad 2.2$$

$$m_f = \frac{f_s}{f_1} \qquad 2.3$$

Where:

$\hat{V}_{modulated}$ – voltage of modulated signal, averaged over one switching period

$\hat{V}_{carrier}$ – voltage of carrier signal, averaged over one switching period

$f_s$ – switching frequency (frequency of carrier signal)

$f_1$ – frequency of modulated signal, same as fundamental frequency of output signal

Frequency modulation ratio should be chosen, depending on the system. Small $m_f$, results in small switching losses but big harmonic distortion. Big $m_f$ lowers the harmonics but increase switch loses. For $m_f \leq 21$ the value of frequency modulation ratio should always be set as an odd integer, since frequencies at which voltage harmonics occur are calculated from equation 2.4 [**33**].

$$f_h = \left(j \cdot m_f \pm k\right) f_1 \; ; \begin{cases} j = 1,3,5, \dots ; k = 0,2,4, \dots \\ j = 2,4,6, \dots ; k = 1,3,5, \dots \end{cases} \tag{2.4}$$

If $m_f$ is set as an integer (odd or equal), the subharmonics are removed from output signal, which lowers THD. If $m_f$ is set as an odd integer it will result in odd symmetry (equation 2.5) and half-wave symmetry (equation 2.6) of output signal. Due to these symmetries, only odd harmonics are present in the signal, thus overall THD is further decreased. Since harmonics for $m_f \leq 9$ are close to fundamental frequency, it is recommended to use higher odd integers. For $m_f > 21$ the harmonics are small enough to use any value of $m_f$ [**33**].

$$f(-t) = -f(t) \tag{2.5}$$

$$f(-t) = -f\left(t + \frac{T_{modulated}}{2}\right) \tag{2.6}$$

The magnitude of voltage $V_t$ in Figure 2.24 depends on the amplitude of modulation frequency. If $m_a \leq 1$ and $m_f > 9$ then RMS value of $V_t$ can be calculated from equation 2.7 [**32**].

$$V_t = m_a \frac{V_{DC}}{2} \tag{2.7}$$

If $m_a > 1$, the converter begins to work in overmodulation. The equation 2.7 is no longer genuine, as the characteristic becomes non-linear. Further increase of $m_a$ will result in switching to square-wave modulation mode, in which the voltage achieved its maximum value and further increase of $m_a$ will not have any results. This is depicted in Figure 2.27 [**33**].

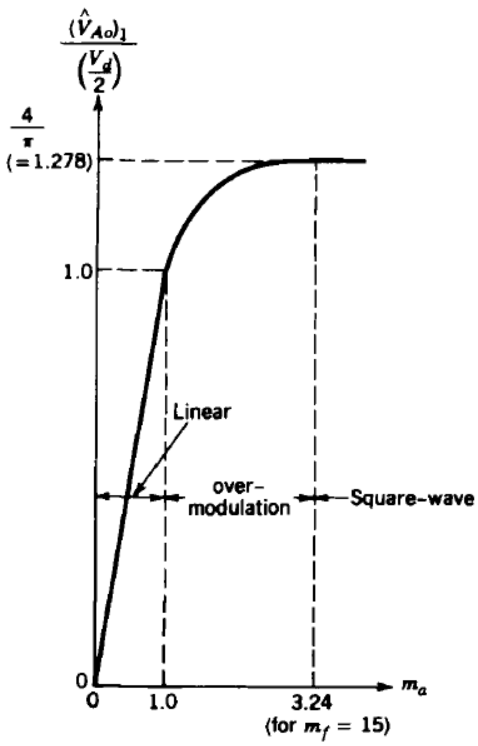


Figure 2.27 $V_t$ as a function of $m_a$ [33]

The output AC voltage $V_t$ is a factor responsible for direction of power flow and amount of transferred active and reactive power. Both $V_t$ and voltage in the AC grid ($V_s$) may be represented as vectors. Figure 2.28 depicts an example of such representation.

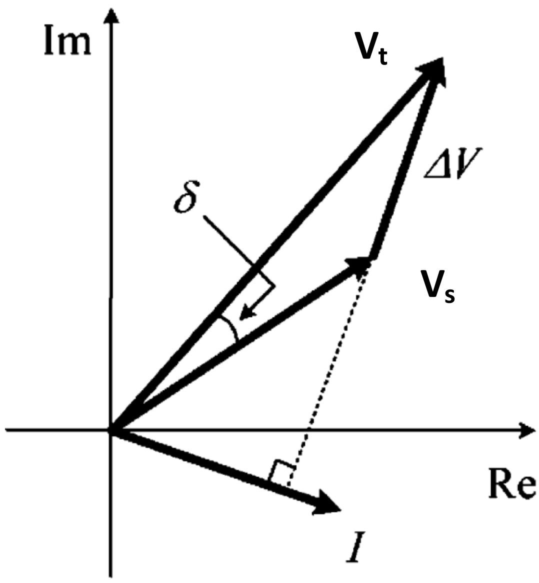


Figure 2.28 Vector representation of grid voltage and AC voltage in VSC [31]

The angle between those 2 vectors in complex plain (δ) is affecting the active power flow, while the difference in vectors magnitude (ΔV) is responsible for reactive power flow. If the phase reactor is simplified to be lossless, then equations 2.8 and 2.9 describe both active and reactive power transmitted to or from AC grid. If the calculated power is positive, then it is transferred from a DC line to the AC grid, as in Figure 2.24. For negative sign, the power is transferred from the AC grid to a DC line.

$$P = \frac{V_t sin\delta}{X_L} V_s \qquad 2.8$$

$$Q = \frac{V_t cos\delta - V_s}{X_L} V_s \qquad 2.9$$

Where:

$X_L$ - reactance of the phase reactor.

### 2.4.4 Non-ideal VSC

The equivalent circuit of one phase non-ideal VSC is depicted in Figure 2.29 [**32**], where variables $V_t'$, $i_p'$ and $i_n'$ represent respectively, terminal voltage on the AC side and DC side currents in non-ideal converter. The following assumptions have been made:

- In conducting state, a diode or a transistor is treated as a resistance ($r_{on}$) in series connection with voltage source ($V_d$), which represents the on-state voltage drop [**32**]
- In blocking state, diodes and transistors are treated as an open circuit
- Turn-on time of transistors and diodes is much shorter than switching signal period, therefore it is simplified to be instant
- Turn-off time of transistors and diodes is much shorter than switching signal period, therefore it is simplified to be instant

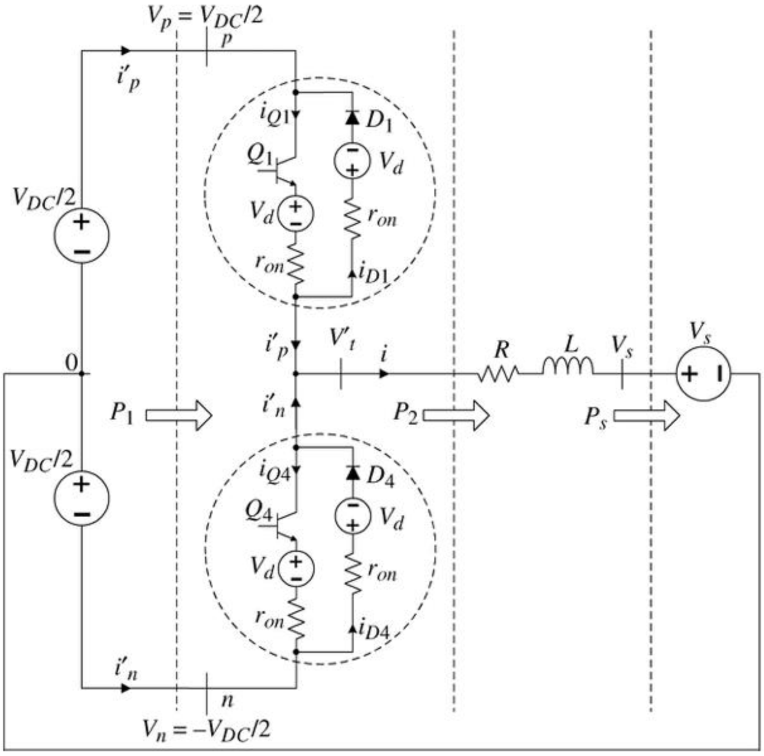


**Figure 2.29 Equivalent circuit of non-ideal VSC [32]**

For this equivalent circuit, the AC voltage at the converter is calculated from equation 2.10

$$V_t' = m_a \frac{V_{DC}}{2} - r_{on} i \tag{2.10}$$

Voltage $\langle V_t' \rangle$ from equation 2.10 should be applied to equations 2.8 and 2.9, in order to obtain more realistic control of active and reactive power transmitted by a DC link. The $r_{on}$ in HVDC is usually much smaller than L, therefore not including it in equations 2.8 and 2.9 will result in a small accuracy drop. [**34**].

### 2.4.5 VSC Configurations

In 2 level configuration, voltage switches rapidly from value $+\frac{V_{DC}}{2}$ to $-\frac{V_{DC}}{2}$, which results in high switching losses at each component [**22**]. In order to decrease those losses, either the switching frequency or the magnitude of switching voltage have to be reduced. Decreasing the switching frequency will decrease switching losses, but at the same time the losses caused by harmonics would increase and the quality of generated AC signal will decrease. Therefore, a 3 level configuration, depicted in Figure 2.30, have been created in order to decrease the magnitude of voltage switch.

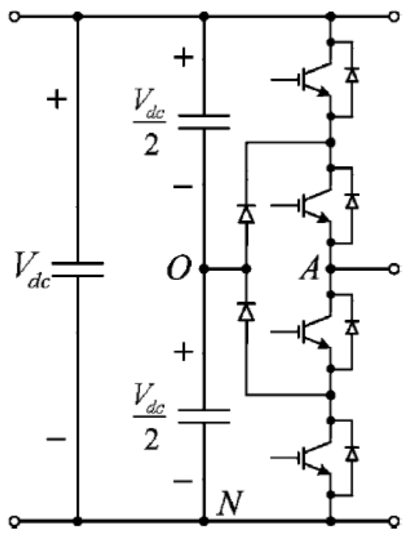


Figure 2.30 Three level VSC topology [31]

In this configuration, an additional output level of 0 V is achieved and the output voltage waveform is depicted in Figure 2.31.

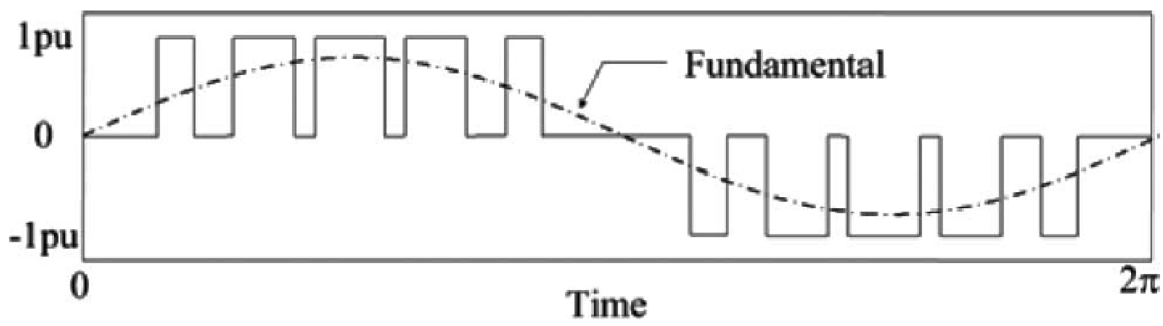


Figure 2.31 Three level VSC output voltage [31]

The switching losses in this configuration have been reduced, due to smaller voltage switch. Higher number of IGBTs in particular configurations results in higher number of voltage levels, thus both switching and harmonic losses would get smaller. Configurations with higher number of levels than 3 are referred as multilevel configurations. Example of obtained AC voltage signal from multilevel converter is depicted in Figure 2.32 while Figure 2.33 presents how THD level changes with number of VSC levels of converter.

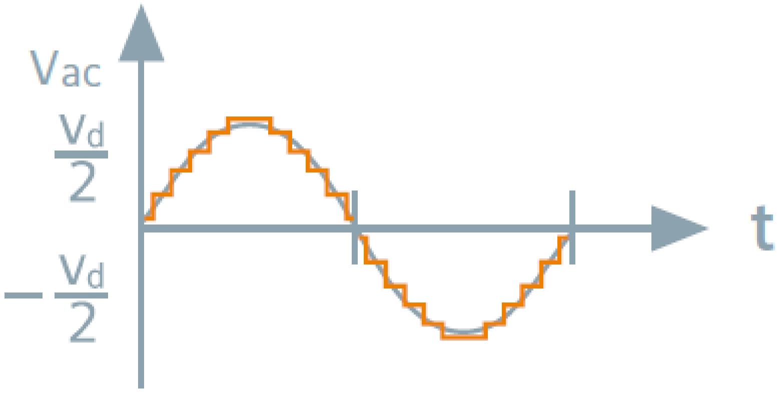


**Figure 2.32 Output AC voltage of multilevel VSC** [35]

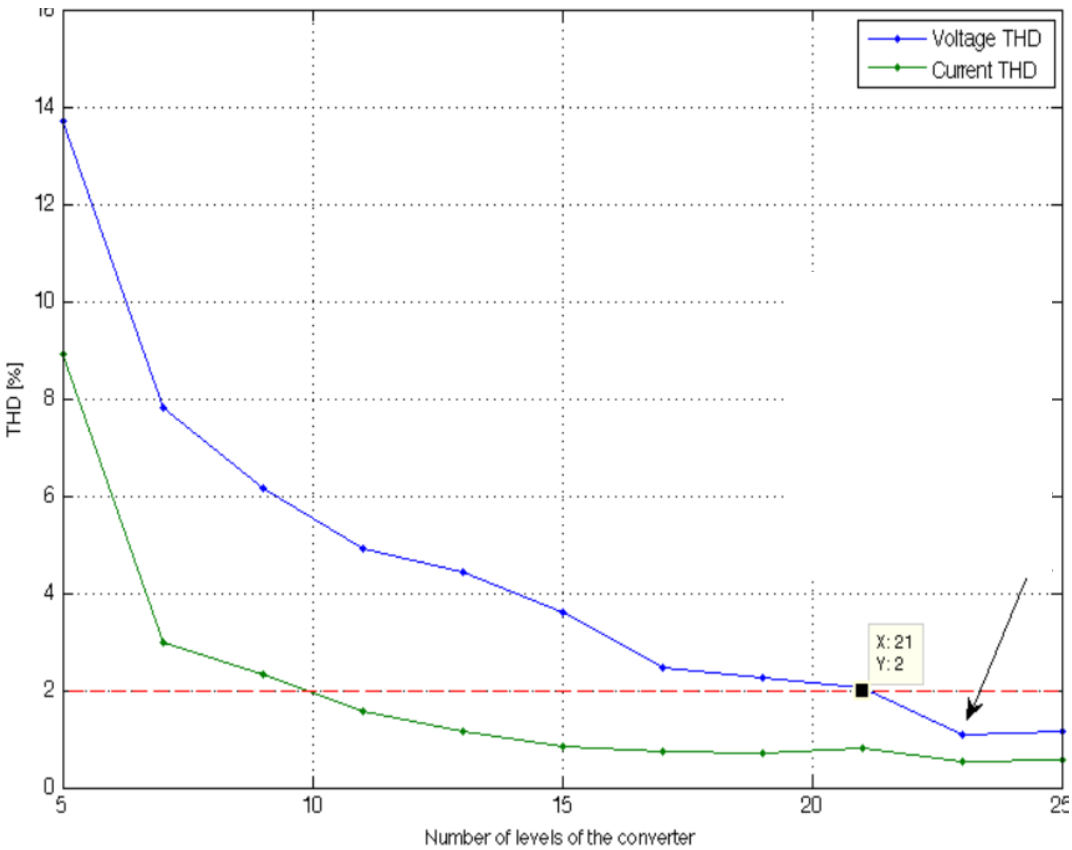


**Figure 2.33 THD level as function of number of levels** [36]

## 2.5 Comparison of Converter Technologies

A comparison of LCC and VSC topologies is shown in Table 2.2.

**Table 2.2 LCC and VSC comparison** [18] [14] [37] [22]

| LCC | VSC |
|---|---|
| Thyristors valves | IGBTs |
| Active power control | Active and reactive power control |
| AC filters required | Small or no AC filters required, due to smaller THD |
| Requires strong AC grid (SC ratio>2) | Can be implemented in weak grids and in islanded mode |
| No Black Start Capability | Capable of Black Start |
| Turn on is controlled, turn off depends on AC grid current | Turn on and turn off are controlled |
| Very high power capability (up to 7200 MW) | Lower power capability than in LCC (1800 MW) |
| Cheapest way of power transmission over very long distances | More expensive than LCC |
| Limited applications in comparison to VSC | Capable of additional applications, such as offshore wind power plants connections |
| Requires big area for converter station | Requires smaller area than LCC for converter station |
| Power flow reversed by change of voltage polarization | Power flow reversed by changing the current flow |

# 3. Control of VSC-HVDC

The control of VSC-HVDC connection is a complicated process, which requires a property referred as "control hierarchy". Control hierarchy consists of 3 control levels, each of them responsible for proper functioning of particular VSC-HVDC connection part [**38**]:

- Lower level control – on which the control system is responsible for things like PWM modulation or balancing voltage across capacitors
- Upper level control – on which the control mode in which converter operates is determined and implemented
- Dispatch control – the highest level, on which the coordination between HVDC stations is implemented

The VSC-HVDC connection model with control hierarchy is represented in Figure 3.1. The idea of control hierarchy is ensuring an easy implementation of changes in control process without the need to build an entire control structure from the beginning.

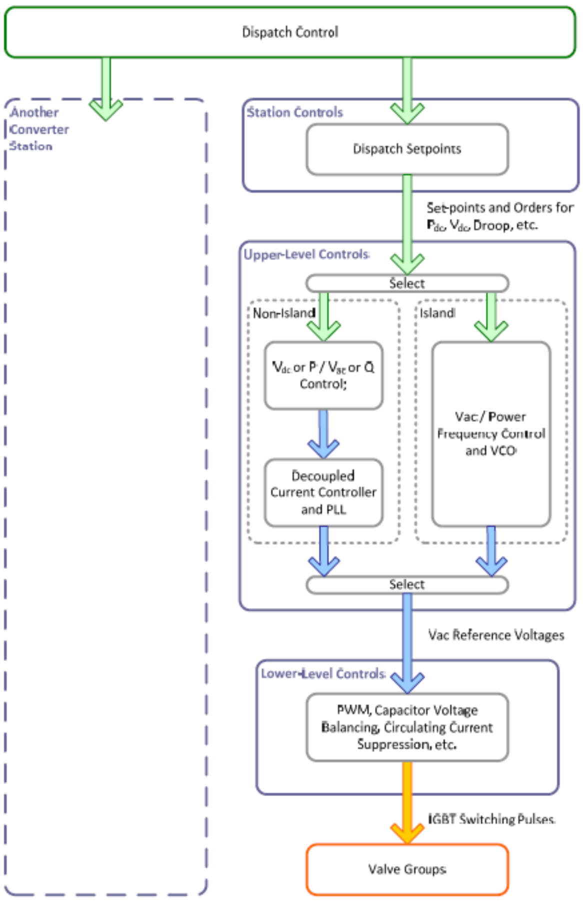


**Figure 3.1 VSC-HVDC model with control hierarchy** [38]

Figure 3.2 depicts a single phase of Modular-Multi-level converter (MMC) [**39**], which is used as an example of slightly more advanced control structure, on which the basic control levels are explained.

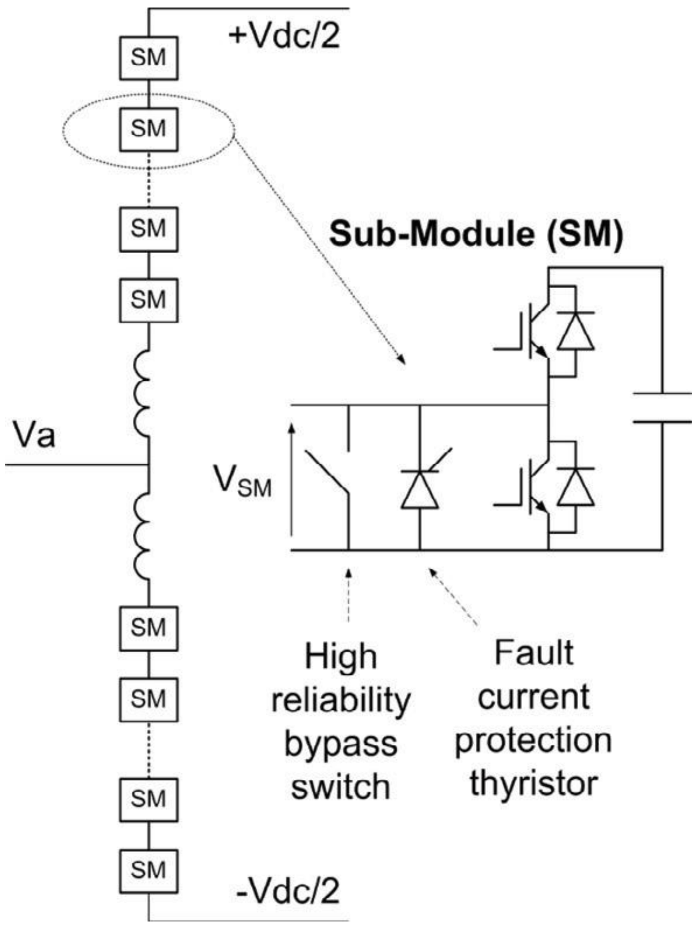


**Figure 3.2 Single Phase of the Modular-Multi-Level Converter [**39**]**

1. **Sub-module control** – The lowest control level, on which the control system is responsible for proper switching of IGBTs in one sub-module. The local over-voltage and over-current protection is also included on this level [**39**].
2. **Phase leg control** – Leg is a connection in Figure 3.2 between $+\frac{V_{DC}}{2}$ and $-\frac{V_{DC}}{2}$, which includes all sub-modules connected to the same phase. This control level is responsible for maintaining the desired AC voltage on the output ($V_a$) and balance the DC voltage across capacitors in each sub-module. It communicates with sub-module control level by sending pulses to each submodule [**39**]. Sub-module control and phase leg control are the lower level controls in MMC.

3. **Converter control** – This level sends control signals to 2nd control level in all 3 phases. It is responsible for obtaining and maintaining the required parameters e.g. DC voltage, AC current, AC voltage, frequency or active and reactive power flow [**39**].
4. **Station control** – This level controls the coordination between converter and other elements in the station, described in section 2.4.1. It is also responsible for protection of all electrical equipment in the station [**39**]. Converter control and station control creates the upper level control of MMC.
5. **System coordination control** – Highest control level, which is responsible for coordination between 2 converter stations, as well as station and the rest of the AC grid [**39**]. This level is the dispatch control level.

The project goal is to determine which control strategy should be applied to converters in MV-MTDC connection for the most reliable coordination between them. Therefore, the scope is focused on upper level control and dispatch control.

## 3.1 Space Phasor and Reference Frames

In order to understand the control strategies and control modes of the VSC, the ideas of space phasor, reference frames and transformation between them have to be presented.

### 3.1.1 $abc$ Reference Frame

In a balanced 3 phase AC system, the instantaneous line-ground voltage or instantaneous phase current may be calculated from the following equations [**32**]:

$$\lambda_a(t) = \lambda_{peak} \cos(\omega t + \varphi) \tag{3.1}$$

$$\lambda_b(t) = \lambda_{peak} \cos\left(\omega t + \varphi - \frac{2\pi}{3}\right) \tag{3.2}$$

$$\lambda_c(t) = \lambda_{peak} \cos\left(\omega t + \varphi + \frac{2\pi}{3}\right) \tag{3.3}$$

Where:

$\lambda_a$, $\lambda_b$, $\lambda_c$ – Line-ground voltage or phase current in phase a,b or c.

$t$ – time

$\lambda_{peak}$ – peak value of voltage or current

$\omega$ – angular frequency

$\varphi$ – initial phase angle (at moment t=0)

Equations 3.1 to 3.3 allow to calculate the values of $\lambda(t)$, $\lambda_b(t)$ and $\lambda_c(t)$ as scalars, but voltage and current may also be represented as vectors. Instead of representing this vector in a traditional Cartesian 2 axis 2 dimensional plane, a 3 axis 2 dimensional plane is used, where angle between each pair of axis is equal 120°. This type of plane is known as $abc$ reference frame and it is depicted in Figure 3.3 [**40**].

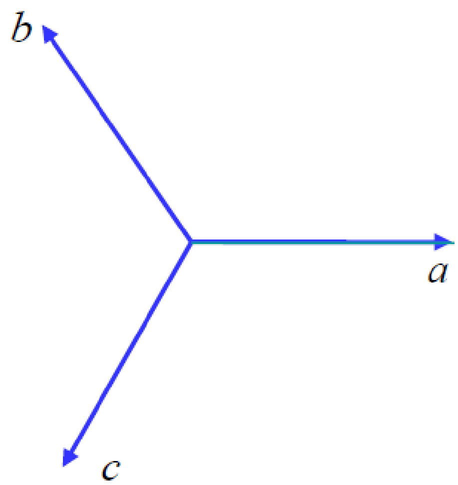


Figure 3.3 An $abc$ reference frame [40]

### 3.1.2 Space Phasor

The new rotating vector $\hat{\lambda}$ is now introduced to $abc$ reference frame. Length of $\hat{\lambda}$ is equal to $\lambda_{peak}$, it's angular frequency $\omega$ is equal to angular frequency of voltages and currents in the AC system and angle between $\hat{\lambda}$ and axis $a$ at time $t = 0$ is equal $\varphi$. By projecting vector $\hat{\lambda}$ on axis $a$ at any time $t$, with example depicted in Figure 3.4, a vector $\lambda_a$ is obtained which length is equal the value of $\lambda_a(t)$ calculated from equation 3.1 [**40**]. Respectively, vectors $\lambda_b$ and $\lambda_c$ which lengths are equal to values calculated from equations 3.2 and 3.3, are obtained by projection of vector $\hat{\lambda}$ on axes $b$ and $c$. This leads to conclusion, that all line-ground instantaneous voltage vectors or all instantaneous phase current vectors at any time $t$ may be graphically represented by a rotating vector $\hat{\lambda}$, which have constant length. This vector is known as a space phasor.

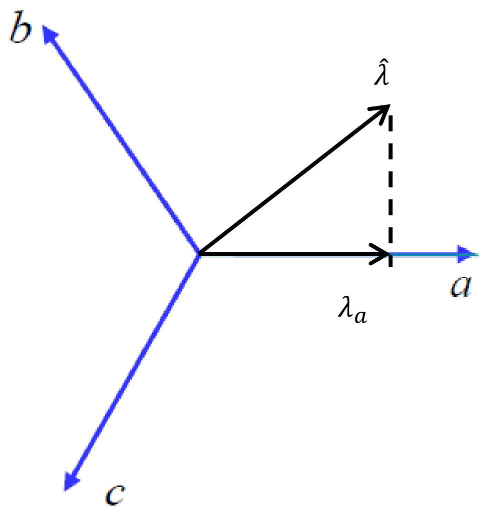


Figure 3.4 Vector $\hat{\lambda}$ and its projection on axis $a$ in $abc$ reference frame [40]

Since $\lambda_a(t)$, $\lambda_b(t)$ and $\lambda_c(t)$ may be calculated from the position of $\hat{\lambda}$ at time $t$, it is possible to reverse the process and determine the position and length of $\hat{\lambda}$ based on instantaneous values. In a balanced 3 phase system, space vector in an $abc$ reference frame ($\hat{\lambda}_{abc}$) is calculated from equation 3.4 [**32**].

$$\hat{\lambda}_{abc}(t) = \frac{2}{3}\left[e^{j0}\lambda_a(t) + e^{j\frac{2\pi}{3}}\lambda_b(t) + e^{j\frac{4\pi}{3}}\lambda_c(t)\right] \qquad 3.4$$

The importance of equation 3.4 comes from the fact that devices used for measurements of voltages or currents in VSC measure instantaneous values. The active and reactive power flow in VSC are dependent on, respectively, the angle and the difference in length between space phasor representing AC voltage at point of common coupling (PCC) and space phasor representing AC voltage at converter terminal. Therefore, by measuring e.g. voltages in all 3 phases in AC grid, it is possible to calculate the space phasor from equation 3.4 and use it as a reference signal in control process.

Use of $abc$ to $space\ phasor$ and vice versa transformation is enough to control a 3 phase balanced AC system. However, it can't be implemented in an unbalanced system [**32**]. This is caused by the fact, that In a balanced system, the output phasor is calculated only from the real component of input vectors (parts which lay on the axes), but in an unbalanced system both real and imaginary components are affecting the output phasor [**32**]. Therefore, in order to improve the control of VSC to cover the fault scenarios when system becomes unbalanced, a transformation to a different reference frames have to be used. The new reference frame is required to have a variable which describes an imaginary part of either voltage or current. There are 2 recommended choices of such reference frame, $\alpha\beta$ reference frame and $dq0$ reference frame.

### 3.1.3 $\alpha\beta$ Reference Frame and $abc$ to $\alpha\beta$ Transformation

This reference frame uses a Cartesian 2 dimension 2 axis coordinate system in a complex plane and is presented in Figure 3.5 [**32**]. Axis α is aligned with the real axis while axis β is aligned with the imaginary axis. The transformation between $abc$ and αβ reference frames is explained below the figure.

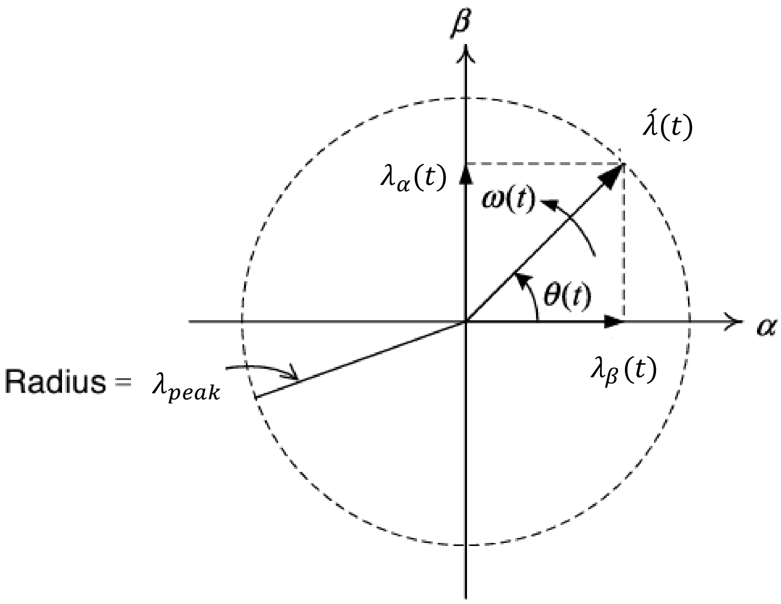


Figure 3.5 αβ reference frame [32]

The space phasor in αβ reference frame ($\hat{\lambda}_{\alpha\beta}$) is calculated from equation 3.5. It is also known that space phasor in one reference frame is always equal the same space phasor in another reference frame, which can be written as equation 3.6 [**40**]. By putting equations 3.4 and 3.5 into equation 3.6, an equation 3.7 is obtained.

$$\hat{\lambda}_{\alpha\beta}(t) = \lambda_\alpha + j\lambda_\beta \tag{3.5}$$

$$\hat{\lambda}_{abc}(t) = \hat{\lambda}_{\alpha\beta}(t) \tag{3.6}$$

$$\frac{2}{3}\left[e^{j0}\lambda_a(t) + e^{j\frac{2\pi}{3}}\lambda_b(t) + e^{j\frac{4\pi}{3}}\lambda_c(t)\right] = \lambda_\alpha + j\lambda_\beta \tag{3.7}$$

Equation 3.7 may be rewritten in a matrix form, thus giving equation 3.8 [**32**] which completes the $abc$ to $\alpha\beta$ transformation.

$$\begin{bmatrix}\lambda_\alpha(t)\\ \lambda_\beta(t)\end{bmatrix} = \frac{2}{3}\begin{bmatrix}1 & -\frac{1}{2} & -\frac{1}{2}\\ 0 & \frac{\sqrt{3}}{2} & -\frac{\sqrt{3}}{2}\end{bmatrix}\begin{bmatrix}\lambda_a(t)\\ \lambda_b(t)\\ \lambda_c(t)\end{bmatrix} \quad 3.8$$

### 3.1.4 $dq0$ Reference Frame and $\alpha\beta$ to $dq0$ Transformation

In $dq0$ reference frame a Cartesian 2 dimension 2 axis coordinate system is used, with axis $d$ aligned with real axis and axis $q$ aligned with imaginary axis. However in contrast to αβ reference frame, where axes are stationary, in $dq0$ reference frame axes are rotating with an angular velocity ε. Figure 3.6 presents the $dq0$ reference frame on abc reference frame [**40**].

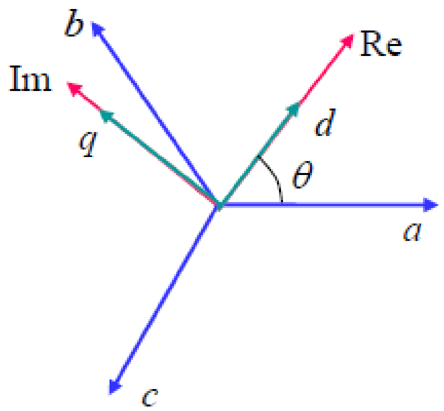


**Figure 3.6 $dq0$ reference frame and abc reference frame** [40]

The benefit of using the $dq0$ reference frame over αβ reference frame is explained on Figure 2.28 and equations 2.8 and 2.9. The equations prove that the active and reactive power flow are dependent on angle between vectors $V_t$ and $V_s$ and the difference in their magnitude. Therefore if real and imaginary axes are stationary, like in Figure 2.28 or in αβ reference frame, the control system have to constantly calculate both angle between $V_t$ and real axis and angle between $V_s$ and real axis, in order to know the value of δ. However if the axes are rotating, like in $dq0$ reference frame, and their angular speed ε is the same as angular speed of space phasors ω, then the vector $V_s$ is always aligned with the real axis and the system needs to calculate only one angle, thus making the calculations easier.

Equation 3.9 shows how the space phasor $\hat{\lambda}_{dq0}$ is calculated in the $dq0$ reference frame. Since $\hat{\lambda}_{dq0}(t)$ = $\hat{\lambda}_{\alpha\beta}(t)$, equations 3.5 and 3.9 may be combined into equation 3.10 [**40**].

$$\hat{\lambda}_{dq0}(t) = (\lambda_d + j\lambda_q)e^{j\varepsilon t} \quad 3.9$$

$$(\lambda_d + j\lambda_q)e^{j\varepsilon t} = \lambda_\alpha + j\lambda_\beta \quad 3.10$$

The equation 3.10 may be rewritten into matrix form, thus becoming equation 3.11 which completes the $\alpha\beta$ to $dq0$ transformation [32].

$$\begin{bmatrix}\lambda_d(t)\\ \lambda_q(t)\end{bmatrix} = \begin{bmatrix}\cos\varepsilon(t) & \sin\varepsilon(t)\\ -\sin\varepsilon(t) & \cos\varepsilon(t)\end{bmatrix}\begin{bmatrix}\lambda_\alpha(t)\\ \lambda_\beta(t)\end{bmatrix} \quad 3.11$$

## 3.2 Upper level Control Strategies

Figure 3.7 presents the schematic diagram of a VSC imposed in the grid. In order to create an upper control model for this structure, the control strategy needs to be chosen first [34]. Control strategy determines which signals are used as input and output in a control process. There are currently 2 control strategies that are used [41]:

- The “Direct power control” strategy, described in section 3.2.1
- The “Vector control” strategy, described in section 3.2.2

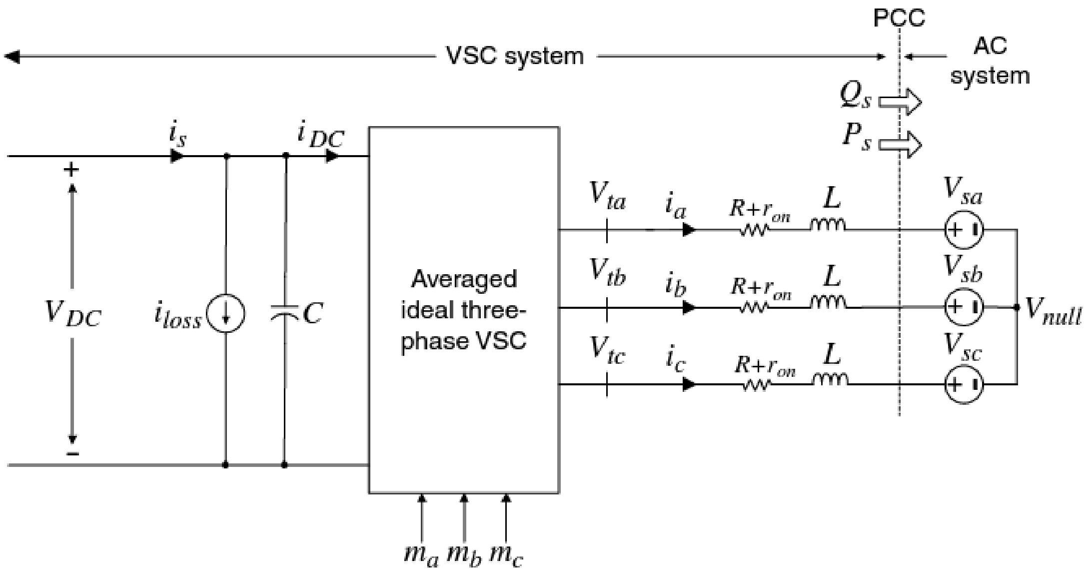


Figure 3.7 Schematic diagram of grid-imposed VSC system [32]

### 3.2.1 Direct Power Control

Direct power control [**41**] is also known as voltage control [**32**] or the $m-\phi$ control [**34**]. In this control strategy 6 signals are used as input, line-ground voltages of the AC grid ( $V_{sa}$, $V_{sb}$ and $V_{sc}$) measured at PCC and voltages at AC terminals of converter ($V_{ta}$, $V_{tb}$ and $V_{tc}$). The control system first calculates the space phasors $V_s$ and $V_t$, then calculates the output signals based on Figure 3.8 [**34**].

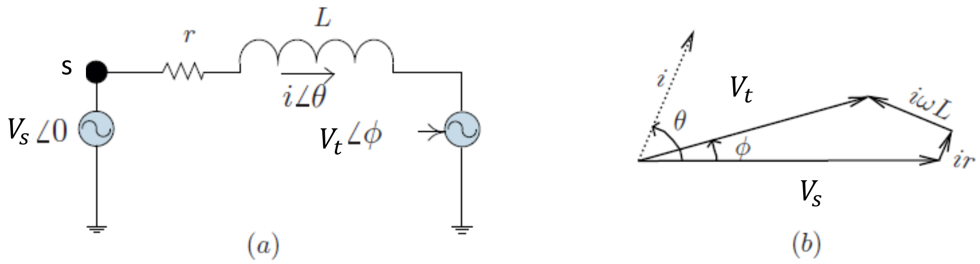


Figure 3.8 Diagram used in Direct Power control strategy [34]

(a) Equivalent circuit
(b) Phasor Diagram

It is presented in equations 2.8 and 2.9 that parameters responsible for the active and reactive power flow are the angle between $V_s$ and $V_t$ (ϕ in Figure 3.8) and the difference in the magnitude of those voltages. Moreover, equation 2.10 proves that magnitude of voltage $V_t$ is dependent on modulation index $m_a$. Therefore, controlling $m_a$ and ϕ will result in direct control of active and reactive power flow (thus names "Direct Power control" and "$m-\phi$" control). This type of control strategy is usually used in Flexible alternating current transmission systems (FACTS) and is easy to implement [**32**]. However, since no currents are measured, this control strategy does not provide the overcurrent protection for converter.

### 3.2.2 Vector Control

Vector Control strategy [**41**] is also known as a current control [**32**], $d-q$ control [**34**] or current vector control [**38**]. In this control strategy, all AC voltages and AC currents are transformed to the $d-q$ reference frame [**34**] and the regulating signals are $i_d$ and $i_q$ [**38**]. This allows the decoupling of active and reactive power flow control, since $i_d$ component controls active power, while $i_q$ component controls reactive power. Figure 3.9 [**34**] depicts the equivalent circuit of VSC in the $dq0$ reference frame, from which the power flow equations are derived.

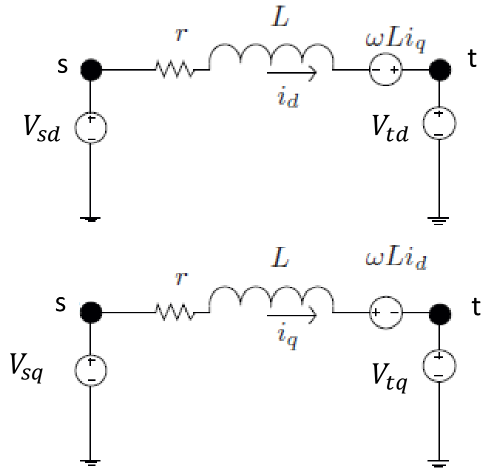


Figure 3.9 Equivalent circuit of VSC in the $dq0$ reference frame [34]

The active power flow is calculated from the top circuit, while reactive power flow is calculated from the bottom circuit. The power flow in this control strategy is calculated from equations 3.12 and 3.13 [**34**]. The voltage $V_{tq}$ does not appear in the equations, since space phasor $V_t$ is always aligned with axis $d$ in the $dq0$ reference frame, thus $V_{tq}$ is always equal to 0.

$$P = \frac{3}{2} V_{td} i_d \tag{3.12}$$

$$Q = -\frac{3}{2} V_{td} i_q \tag{3.13}$$

Vector Control is more complex than Direct Power Control, however there are numerous advantages of this method, such as [**32**]:

- Overcurrent protection
- Robustness against variations in parameters of both VSC and AC grid
- Superior dynamic performance
- Higher control precision

Due to those advantages, this control strategy was implemented in the project.

## 3.3 Non-islanded Control Modes

A control mode determines which parameters of an HVDC connection (e.g. DC voltage, AC voltage, active power, reactive power etc.) are regulated by a VSC terminal. As shown in Upper-level controls block in Figure 3.1, VSC converters may operate in one of islanded or non-islanded control modes. The non-islanded control modes are modes implemented in VSC terminals connected to AC grids with strong synchronous generation [**38**]. There are 3 non-islanded control modes [**8**]:

- Fixed power flow (also known as $PQ$ control)
- Constant DC voltage (also known as $U_{DC}$ control)
- DC voltage droop control (also known as $U_{DC}$ droop control)

Figure 3.10 depicts graphical representation of those 3 modes, which are described in sections 3.3.1 to 3.3.3.

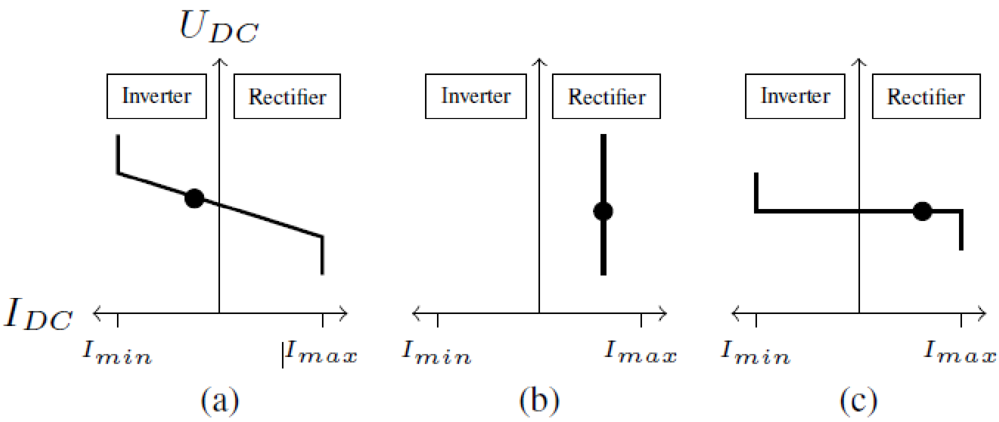


**Figure 3.10 Basic modes of VSC terminal controls** [8]

**(a) – DC Voltage droop control**
**(b) – Fixed power flow**
**(c) – Constant DC voltage**

### 3.3.1 Fixed Power Flow

In this mode, converter has to maintain the fixed flow of both active and reactive power. This is visible in Figure 3.10 (b), where current remains constant while voltage changes freely. Figure 3.11 depicts the block diagram of active power control and Figure 3.12 depicts reactive power control block diagram. The $PI$ block in both figures represents the PI controller, the symbols with asterisk represent the reference signal and the current ramps ensures that the overcurrent would not occur with $i_{d,max} = i_N$ and $i_{q,max} = \sqrt{{i_N}^2 - {i_d}^2}$ [**34**].

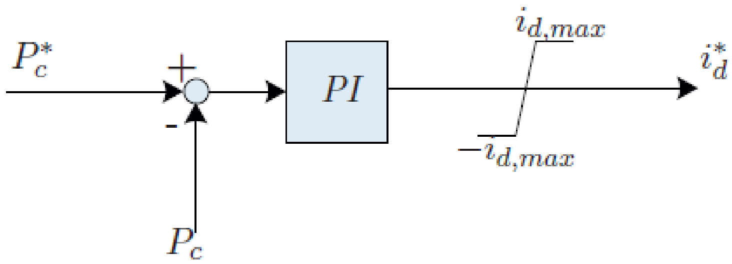


Figure 3.11 Block diagram of active power control [34]

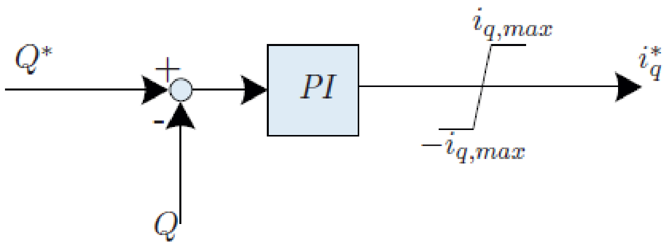


Figure 3.12 Block diagram of active power control [34]

### 3.3.2 Constant DC Voltage

Opposite to fixed flow, in this mode converter has to maintain the constant DC voltage level, while current can change freely (and so can active and reactive power flow) as depicted in Figure 3.10 (c). Figure 3.13 depicts the block diagram for constant DC voltage control mode. The functions of $PI$ block, symbols with asterisk and current ramp are the same as in Fixed flow control. In this mode, $i_q^* = i_q$, therefore the reactive power is not controlled [**34**].

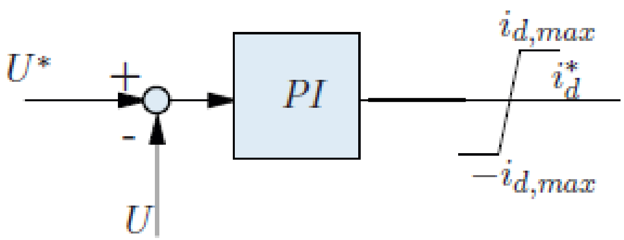


Figure 3.13 Block diagram of constant DC voltage [34]

### 3.3.3 DC Voltage Droop Control

In this control mode, neither power flow nor DC voltage is a fixed value. As shown in Figure 3.10 (a), the VSC is responsible for maintaining the DC voltage, depending on the current or active power that flows through it. Equation 3.14 shows the general droop control formula [**8**]

$$\chi = \chi_{ref} - \frac{1}{k_{DC}}(U_{DC} - U_{DC\_ref}) \quad 3.14$$

Where:

$\chi$ – Power or current which flows through converter

$\chi_{ref}$ – reference current or reference power that is supposed to be achieved and maintained

$k_{DC}$ – droop coefficient, it determines the steepness of slope in Figure 3.10 (a).

This formula can also describe fixed power flow and constant DC voltage modes. In first case, droop coefficient $k_{DC} = \infty$ while in second case $k_{DC} = 0$. Therefore, these 2 modes are sometimes referred as particular cases of droop control. [**8**] Figure 3.14 depicts the block diagram of DC voltage droop control [**34**].

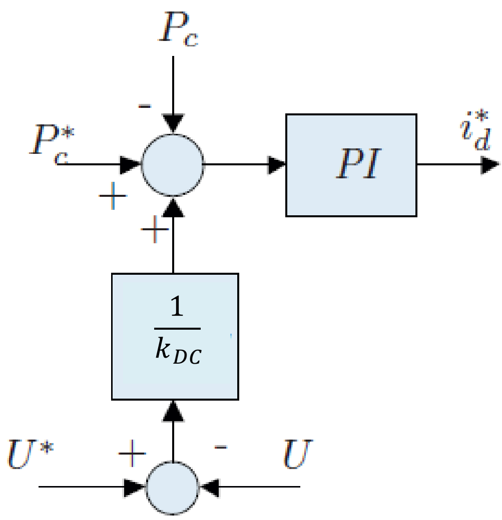


**Figure 3.14 Block diagram of DC voltage droop control** [34]

Figure 3.10(a) have depicted the most basic droop control characteristic, but there are more advanced types of DC voltage droop control. Figure 3.15 depicts 4 examples of such control modes [**8**]. For those types of control, the block diagram becomes much more complicated. In this project, only the basic type of DC voltage droop control will be implemented.

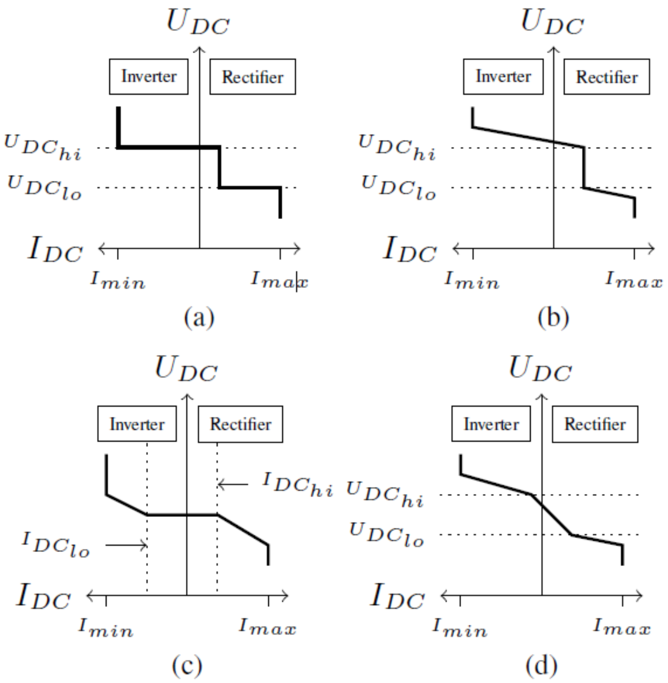


**Figure 3.15 Advanced droop control examples [8]**

**(a) – voltage margin method**
**(b) – constant current dead-band**
**(c) – constant voltage dead-band**
**(d) – undead-band**

## 3.4 Islanded Control Mode – AC Voltage and Frequency

The islanded control modes are implemented in converters that are connected to a weak AC grid with synchronous generation, AC grid with asynchronous generation or AC grid with disconnected load [**38**]. Examples of islanded control modes are:

- Frequency droop control
- AC voltage control
- AC voltage droop control

In the project, an islanded control mode was implemented for terminal connected to an offshore wind farm. Based on informations from [**38**] and [**42**], the implemented mode should be responsible for control of the terminal AC voltage $V_t^*$ and frequency of the AC grid connected to a VSC converter. Figure 3.16 shows the block diagram of $V_{ac}$-f control, on which the created control mode model is based [**38**].

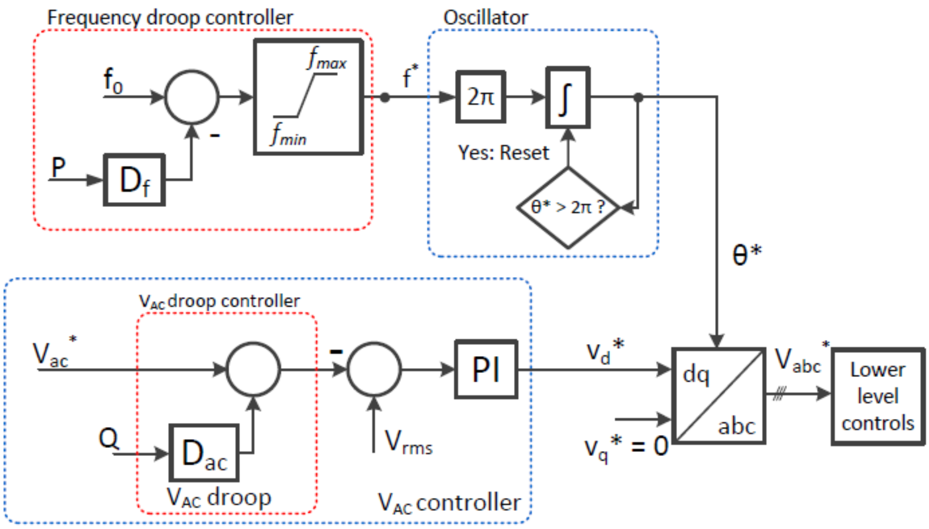


Figure 3.16 Block diagram of $V_{ac}$-f control [38]

## 3.5 Inner control loop

Regardless of control mode in which VSC is operating, the output signal is always $i_d^*$ or $i_q^*$, however Lower Level Controls require the reference voltage phasor $V_t^*$ as an input signal. Decoupled current controller, presented in Figure 3.17 [34] is used to obtain the $V_t^*$ phasor from $i_d^*$ and $i_q^*$ values and ensure that change in one of currents will not cause a transient in the other one [38].

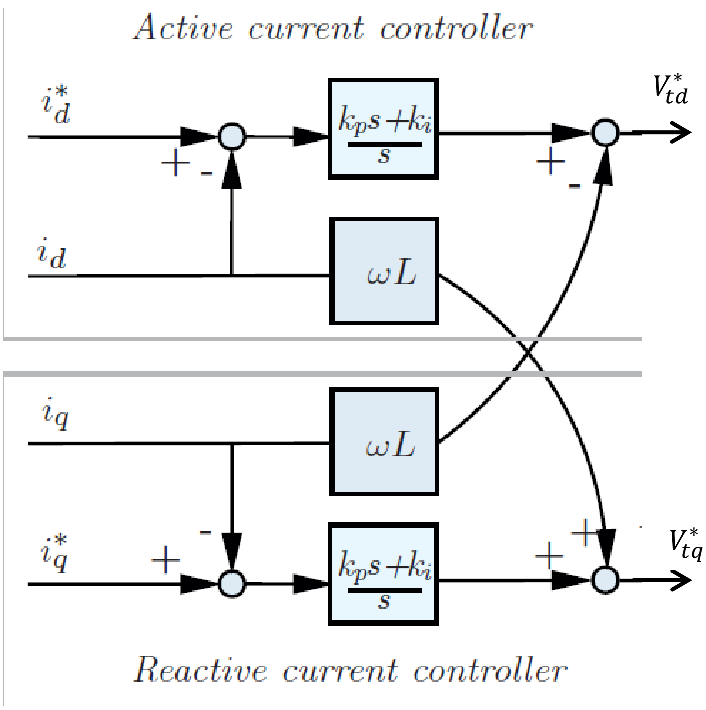


Figure 3.17 Block diagram of inner control loop [38]

## 3.6 Dispatch Controls

Dispatch controls may be defined as a control level which determines in what control mode should every VSC work in an HVDC connection and what are the values of reference parameters (e.g. voltage, power, frequency) that will be used as input signals for Upper-level controls [**38**]. In other words, dispatch controls are responsible for proper coordination of an HVDC connection.

### 3.6.1 PtP Dispatch Controls

In Point-to-Point connection between 2 strong AC grids, there are 3 control modes that may be implemented as Upper-Levels controls for both converters. These are Fixed Flow, Constant DC voltage and DC voltage droop. Since one converter is working as a rectifier and the other as an inverter, this resulting in 9 possible configurations of dispatch control. Table 3.1 presents all 9 control configurations and comments regarding their performance [**34**].

**Table 3.1 Control configurations for PtP HVDC connection** [34]

| | Control modes | | |
|---|---|---|---|
| No. | Rectifier | Inverter | Remarks |
| 1 | Constant power | Constant power | Not viable |
| 2 | Constant power | dc droop | Viable but with risk of dc over voltage |
| 3 | Constant power | Constant dc voltage | Viable but with risk of dc over voltage |
| 4 | dc droop | Constant power | Good performance, Power flow control by inverter |
| 5 | dc droop | dc droop | Good performance, Power flow control by both |
| 6 | dc droop | Constant dc voltage | Ok, Power flow control by rectifier |
| 7 | Constant dc voltage | Constant power | Good performance, Power flow control by inverter |
| 8 | Constant dc voltage | dc droop | Ok, power flow control by inverter |
| 9 | Constant dc voltage | Constant dc voltage | Not viable |

The table shows that both converters can't work in Fixed power flow mode (situation 1) or in Constant DC voltage mode (situation 9) at the same time, since in these situations, the system becomes unstable in a steady-state operation [**34**]. The other configurations may be implemented, since the system is stable in steady-state. However the overvoltage may occur in configurations 2 and 3 in an event where the inverter VSC can't transfer power to a connected AC grid, while rectifier

VSC still transfers power. Thus, configurations from 4 to 8 are recommended for Dispatch control in PtP connection [**34**].

### 3.6.2 MTDC Dispatch Controls

In an MTDC connection with big number of connected VSCs, and where some of them might work in an islanded mode, the number of possible dispatch control modes is very big. However by assuming that all converters work in a non-islanded mode and taking Table 3.1 into consideration, the number of dispatch controls is reduced to 3 control modes [**34**]:

1. **Master-slave control** – in this control mode, one VSC operates in a constant DC voltage mode and is referred as master terminal, while other terminals, which are called slaves, operate in the Fixed power flow mode. This control mode has 2 major drawbacks. First, in an MTDC connection with a large number of connected terminals, the fault in any slave terminal may cause a big deviation in power flow between master terminal and AC grid to which it is connected. Second, when fault occurs in a master terminal, one of slave terminals must become the new master, otherwise the system will become unstable [**8**]. Due to those drawback, this method is not recommended for MTDC operation [**34**].
2. **DC droop control** – in this mode, at least 2 converters work in DC voltage droop control, while other works in fixed power flow. Since several converters are responsible for maintaining the DC voltage level, the fault in any converter distributes the burden on all of them [**8**]. Even if fault occurs in one of converters responsible for DC droop control, the other converters are still capable of maintaining the desired DC voltage level. [**34**]
3. **Master-slave with droop control** – in this mode, one converter operates in a constant DC voltage mode, at least one converter operates in a DC voltage droop control and other converters operates in a fixed power flow mode. During normal operation of the grid, DC voltage is controlled by a master terminal. However, if fault occurs in any terminal, the impact is distributed on both master terminal and all terminals that operates in a DC voltage droop control. Additionally, if fault occurs in a master terminal, terminals that operates in a droop control will maintain voltage level in the DC grid.

# 4. COBRAcable Model and Control Strategies Implementation

The theoretical knowledge presented in chapter 2 is applied to create generic models of a COBRAcable, both as a PtP and an MTDC connection. These models were created in a DIgSILENT Power Factory 2016 and their visual representations, along with implemented data, are presented in subchapters 4.1 and 4.2 respectively. Subchapter 4.3 presents the control models, created with DIgSILENT Simulation Language (DSL).

## 4.1 PtP Model

Figure 4.1 presents the visual representation of a PtP connection's generic model, created in the DIgSILENT Power Factory. In the model, elements that lay on the left side of the red line represents the electrical equipment of an HVDC substation in Eemshaven (Netherlands), along with ½ of both positive (top) and negative (bottom) DC voltage cables. The elements on the right side of the line represents the second halves of DC cables and the equipment of an HVDC substation in Endrup (Denmark). Figure 4.2 presents the magnified left half of Figure 4.1, along with names of visible elements. Description of those elements and the data implemented in them are presented in sections 4.1.1 to 4.1.5. Due to the project limitations, some data were not accessible (e.g. short circuit power of external grid) while other data were not required (e.g. data regarding harmonics). In those cases, the default values given in Power Factory were used.

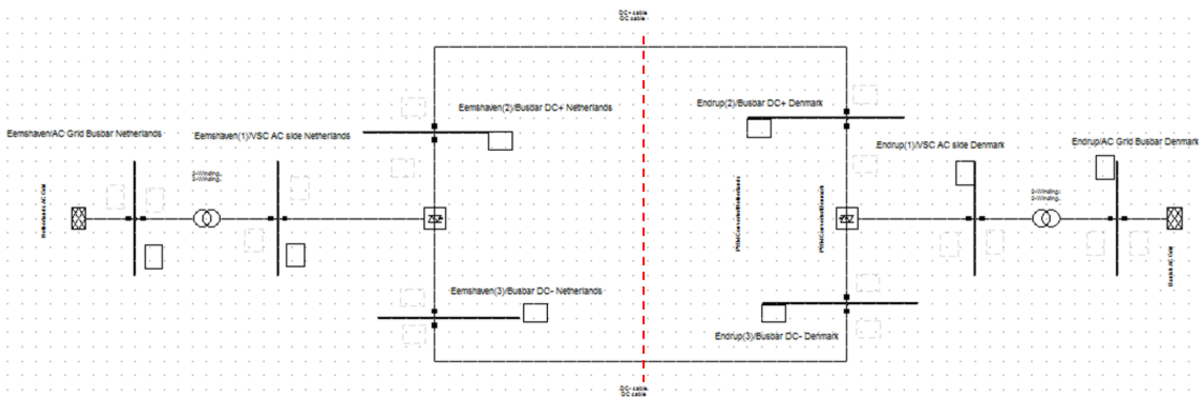


Figure 4.1 Visual representation of a PtP generic model

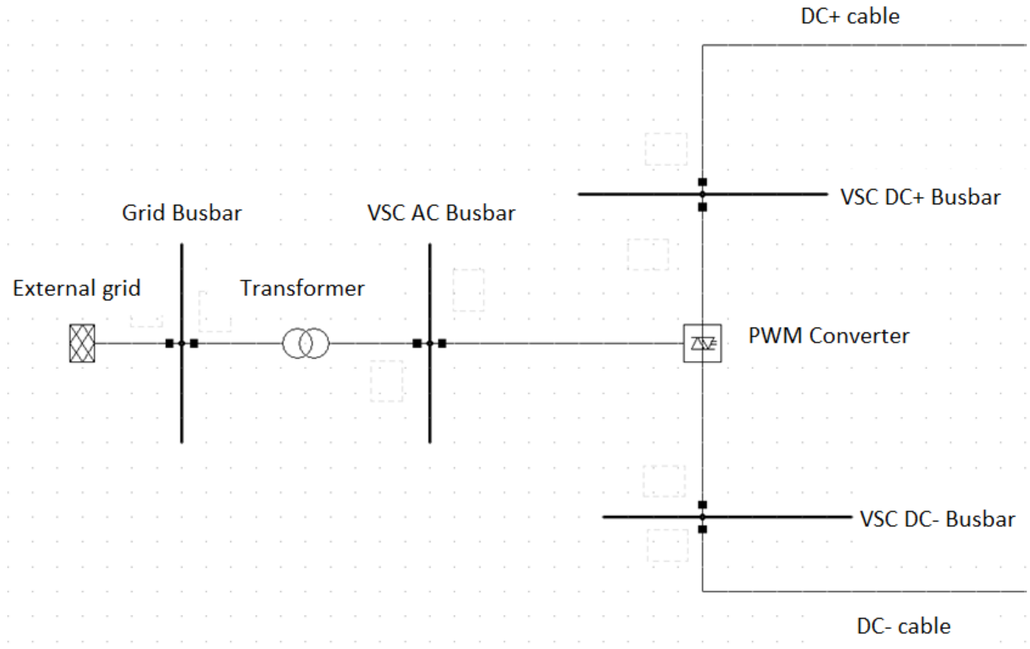


Figure 4.2 Elements of PtP connection

### 4.1.1 External Grid

The external grid symbol represents the AC grid to which the HVDC substation is connected. Table 4.1 presents the data implemented in both external grids. The 4th column in the table shows which reference or formula were used to obtain the given value. The "Default Value" means that the value was implemented as default in Power Factory.

Table 4.1 External Grid data

| Parameter [unit] | Danish grid | Netherlands grid | Reference |
|---|---|---|---|
| Bus type | Slack | Slack | [42] |
| Angle [deg] | 0 | 0 | [42] |
| Voltage Setpoint [p.u] | 1 | 1 | [42] |
| Short Circuit Maximum Power [MVA] | 10000 | 10000 | Default value |
| Short Circuit Maximum Current [kA] | 14.43376 | 15.19343 | Calculated by power factory |
| R/X ratio | 0.1 | 0.1 | [43] |
| C factor | 1.1 | 1.1 | [43] |

### 4.1.2 Transformer

The transformer symbol represents a 3 phase 2-winding voltage transformer. Table 4.2 presents the data implemented in PtP model's transformers. The rated voltage for LV side of transformer have to be the same as rated RMS Line-Line voltage of PWM Converter. In order to maintain the linear characteristic of voltage (Figure 2.27) the modulation index $m_a$ should be chosen between 0.9 and 1.0. The rated voltage value is calculated from equation 4.1 [**43**].

**Table 4.2 Transformer data**

| Parameter [unit] | Danish transformer | Netherlands transformer | Reference |
|---|---|---|---|
| Rated Power [MVA] | 700 | 700 | [**10**] |
| Frequency [Hz] | 50 | 50 | [**10**] |
| Rated Voltage – HV side [kV] | 400 | 380 | [**10**] [**9**] |
| Rated Voltage – LV side [kV] | 370 | 370 | Equation 4.1 |
| Positive Sequence Reaction [p.u] | 0.11 | 0.11 | [**42**] |
| Copper losses [kW] | 250 | 250 | [**42**] |

$$V_t = \frac{\sqrt{3}}{2\sqrt{2}} \cdot m_a \cdot U_{DC} = \frac{\sqrt{3}}{2\sqrt{2}} \cdot 0.9 \cdot 640\ kV \approx 370\ kV \qquad 4.1$$

### 4.1.3 PWM Converter

The PWM Converter symbol represents a Modular Multilevel Converter (MMC) with modules operating in a half bridge configuration [**43**]. The topology of such converter is depicted in Figure 4.3. Table 4.3 presents the data implemented in PWM Converters in the model. The arm reactor inductance was found from plot presented in Figure 4.4. The plot was created based on data from [**38**]. The submodule capacitance was calculated by using equation 4.2, with the assumptions that the energy stored in each submodule is 40 kJ/MVA [**38**] and that the voltage across capacitor ($v_c$) is the same for all submodules [**38**].

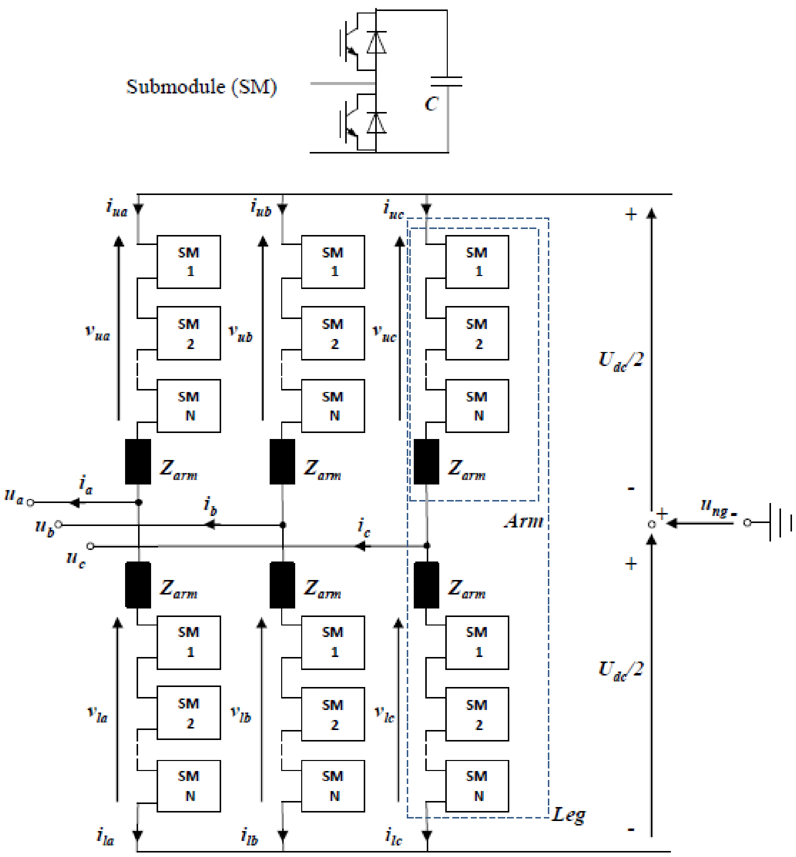


Figure 4.3 Topology of MMC [43]

Table 4.3 PWM Converter Data

| Parameter [unit] | Danish Converter | Netherlands Converter | Reference |
|---|---|---|---|
| Rated AC voltage [kV] | 370 | 370 | Equation 4.1 |
| Rated DC voltage [kV] | 640 | 640 | [10] |
| Rated Power [MVA] | 700 | 700 | [10] |
| Arm Reactor Inductance [mH] | 33 | 33 | Figure 4.4 |
| Submodule Capacitance [mF] | 4.6 | 4.6 | Equation 4.2 |
| Number of submodules per arm | 200 | 200 | [38] |
| No-load lossess [kW] | 3000 | 3000 | [42] |

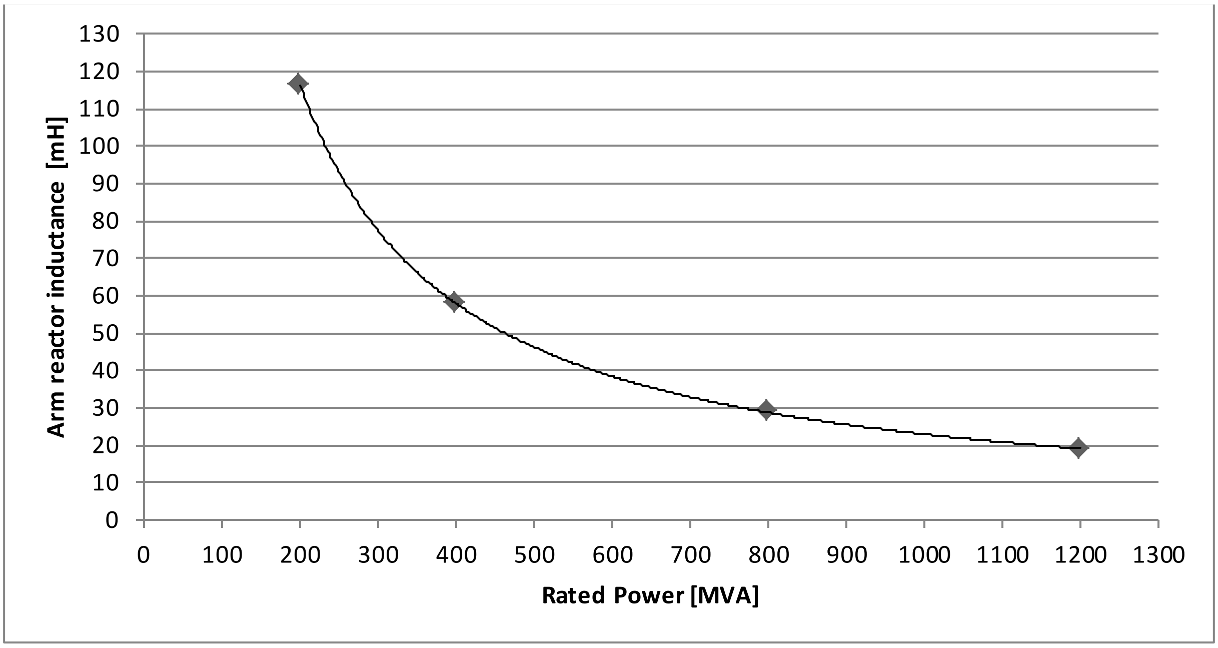


Figure 4.4 Arm reactor inductance as a function of Rated Power

$$C = \frac{2 \cdot S \cdot E_{SM}}{6 \cdot N_a \cdot v_c} = \frac{2 \cdot 700\ MVA\ \cdot 40\ \frac{kJ}{MVA}}{6 \cdot 200 \cdot \left(\frac{640\ kV}{200}\right)^2} = 4.6\ mF \qquad 4.2$$

Where:

$C$ – Capacitance of sub-module

S – Rated Power

$E_{SM}$ – Energy stored in submodule

$N_a$ – Number of sub-modules per arm

$v_c$ – Voltage across submodule

### 4.1.4 Busbars

The Busbar symbol represent a terminal to which 2 or more objects are connected. All busbars on the left side represents terminals in Eemshaven substation, while all terminals on the right are located in Danish substation. Table 4.4 presents the data regarding busbars.

Table 4.4 Busbar Data

| Parameter [unit] | Grid Busbar | VSC AC Busbar | VSC DC + Busbar | VSC DC- Busbar |
|---|---|---|---|---|
| System type | AC | AC | DC | DC |
| Phase Technology | ABC | ABC | - | - |
| Rated Voltage [kV] | Netherlands – 380<br>Denmark – 400 | 370 | +320 | -320 |

### 4.1.5 DC Submarine Cables

The lines which connects both substations are representation of DC submarine cables. Table 4.5 presents the data implemented into DC cables. The cross section and resistance per km were both found in [**44**].

Table 4.5 DC Cables data for PtP

| Parameter [unit] | DC Cable | Reference |
|---|---|---|
| Rated Voltage [kV] | 320 | [**10**] |
| Rated Current [kA] | 1.0938 | $I_{DC} = \frac{P_{DC}}{2U_{DC}}$ |
| Cable/OHL | Cable | [**10**] |
| System type | DC | [**10**] |
| Conductor Material | Copper | [**38**] |
| Cross section [$mm^2$] | 800 | **Błąd! Nie można odnaleźć ródła odwołania.** |
| Resistance per km [Ω/km] | 0.0221 | **Błąd! Nie można odnaleźć ródła odwołania.** |
| Length [km] | 350 | [**10**] |

## 4.2 MTDC Model

In the next step, PtP generic model is expanded into an MTDC model. Figure 4.5 depicts the visual representation of the MTDC model, created in DIgSILENT Power Factory. Expanding PtP to a 3 terminal MTDC connection resulted in 2 major changes in the model. First change is the creation of 3rd HVDC substation, which is depicted inside the red rectangle in Figure 4.5. This substation is not connected to the AC grid, but to the offshore wind farm, which magnified symbol is depicted in Figure 4.6. More detailed description of wind farm element and data implemented into it are presented in section 4.2.1, while data regarding other elements of offshore substation are located in section 4.2.2. Second change in the model is creation of 2 additional busbars, located inside green rectangle. These busbars represent a marine hub, which serves as a central point in an MTDC grid build in star topology (depicted and described in section 2.2.5). Due to its existence, the existed DC cables required some modification, as well as 2 new cables appeared. Marine hub and DC cables changes are described in section 4.2.3. In the tables, the value ”assumed’ appear in reference column. This value means that the values were agreed upon on supervisor meetings.

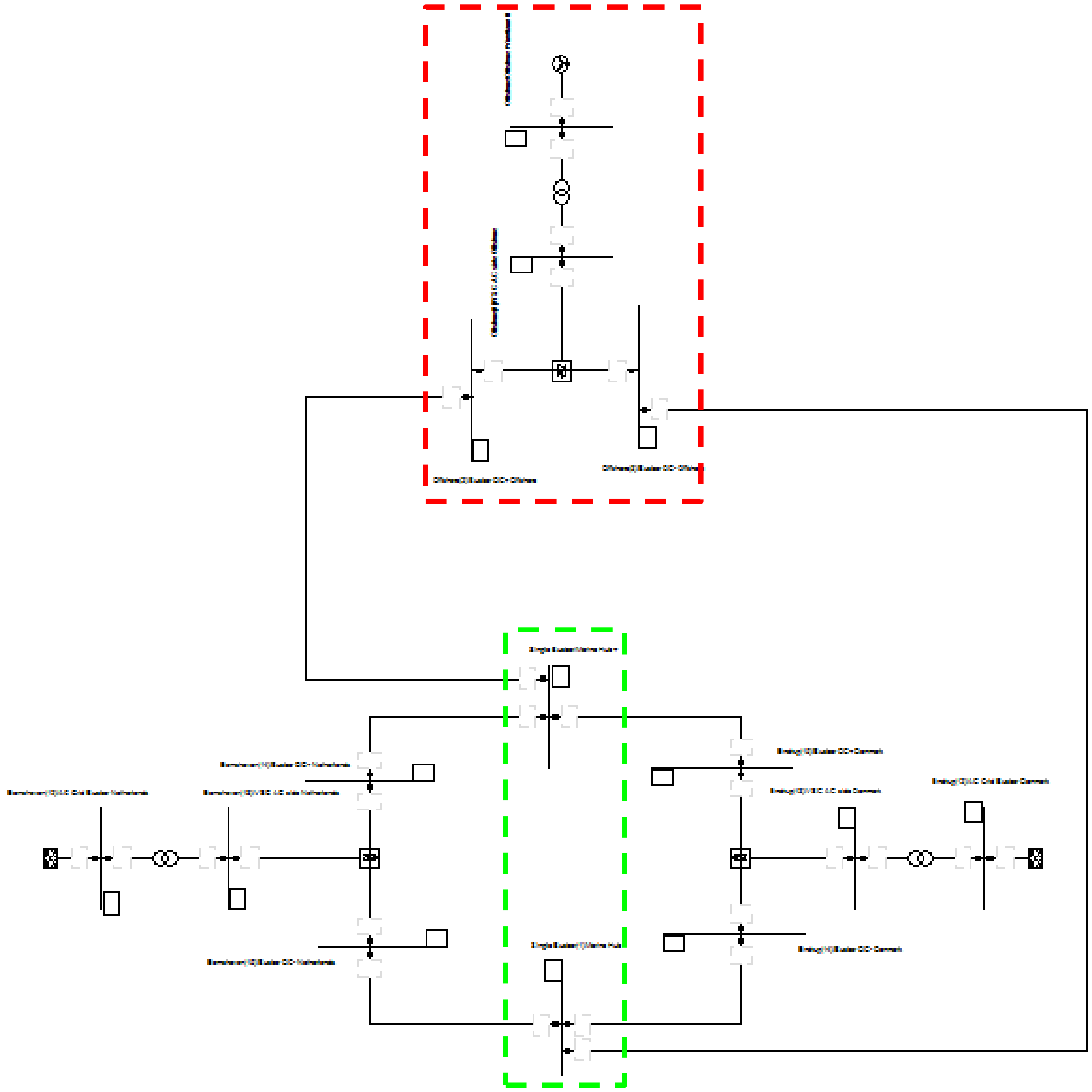

Figure 4.5 Visual representation of the MTDC model

### 4.2.1 Offshore wind farm

The symbol depicted in Figure 4.6 is a “Static Generator” and it represents an offshore wind farm, located in the north sea. Data implemented in the model are depicted in Table 4.6. As in previous tables, the only data presented in this section are data which are constant, regardless of simulation.

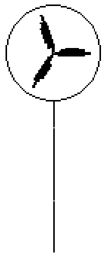

Figure 4.6 Wind farm symbol

Table 4.6 Offshore wind farm data

| Parameter [unit] | Offshore wind farm | Reference |
|---|---|---|
| Technology | 3PH | [**42**] |
| Plant Category | Wind | [**42**] |
| Nominal Apparent Power [MVA] | 700 | Assumed |
| Power factor | 0.8 | Default value |
| Input mode | P,Q | [**42**] |

### 4.2.2 Offshore substations elements

Apart from the offshore windfarm, the description of other elements of 3rd substation, such as transformer or PWM converter, is the same as in subchapter 4.1. Data regarding those elements are presented in tables, from Table 4.7 to

Table 4.9.

Table 4.7 Offshore transformer data

| Parameter [unit] | Offshore transformer | Reference |
|---|---|---|
| Rated Power [MVA] | 700 | Assumed |
| Frequency [Hz] | 50 | Assumed |
| Rated Voltage – HV side [kV] | 370 | Equation 4.1 |
| Rated Voltage – LV side [kV] | 150 | Assumed |
| Positive Sequence Reaction [p.u] | 0.11 | [**42**] |
| Copper losses [kW] | 250 | [**42**] |

Table 4.8 Offshore PWM Converter Data

| Parameter [unit] | Offshore Converter | Reference |
|---|---|---|
| Rated AC voltage [kV] | 370 | Equation 4.1 |
| Rated DC voltage [kV] | 640 | [**10**] |
| Rated Power [MVA] | 700 | Assumed |
| Arm Reactor Inductance [mH] | 33 | Figure 4.4 |
| Submodule Capacitance [mF] | 4.6 | Equation 4.2 |
| Number of submodules per arm | 200 | [**38**] |
| No-load losses [kW] | 3000 | [**42**] |

**Table 4.9 Offshore Busbar Data**

| Parameter [unit] | Wind farm Busbar | VSC AC Busbar | VSC DC + Busbar | VSC DC- Busbar |
|---|---|---|---|---|
| System type | AC | AC | DC | DC |
| Phase Technology | ABC | ABC | - | - |
| Rated Voltage [kV] | 150 | 370 | +320 | -320 |

### 4.2.3 Marine Hub and DC Cables

The marine hub is the key structure in star topology MTDC. It allows the functioning of an MTDC network in case of a converter loss. If the DC voltage level of some converters are not the same, the DC/DC converters may be located in a marine hub. In created model, the marine hub does not need any additional converters. It is represented as 2 DC busbars, one for rated voltage +320 kV and one for -320 kV. The marine hub is located on the path of a DC cables from PtP model, 250 km away from Netherlands, 100 km away from Denmark and 70 km away from offshore wind farm.

## 4.3 Control Modes Models

The generic models presented in Figure 4.1 and Figure 4.5 are sufficient for a load flow and a short circuit tests. However, in order to perform an RMS or EMT analysis, the PWM converters requires a predefined controller system, that will determine system's behaviour. The control modes models have been created by using a DIgSILENT Simulation Language (DSL). Section 4.3.1 contains a brief explanation of how to build a model in DSL (more detailed explanation can be found in [**45**]). Sections 4.3.2 to 4.3.6 describes the created control models, based on control loops presented in subchapters

3.3, 3.4 and 3.5. In the course of the project, it was determined that since the MTDC connection focuses mainly on active power flow and maintain of Udc, the reactive power control shall be skipped.

### 4.3.1 DIgSILENT Simulation Language

The system modelling in DSL is based on 5 elements. Figure 4.7 depicts the interconnections between those elements, while the elements are described in more detail below the figure [**45**].

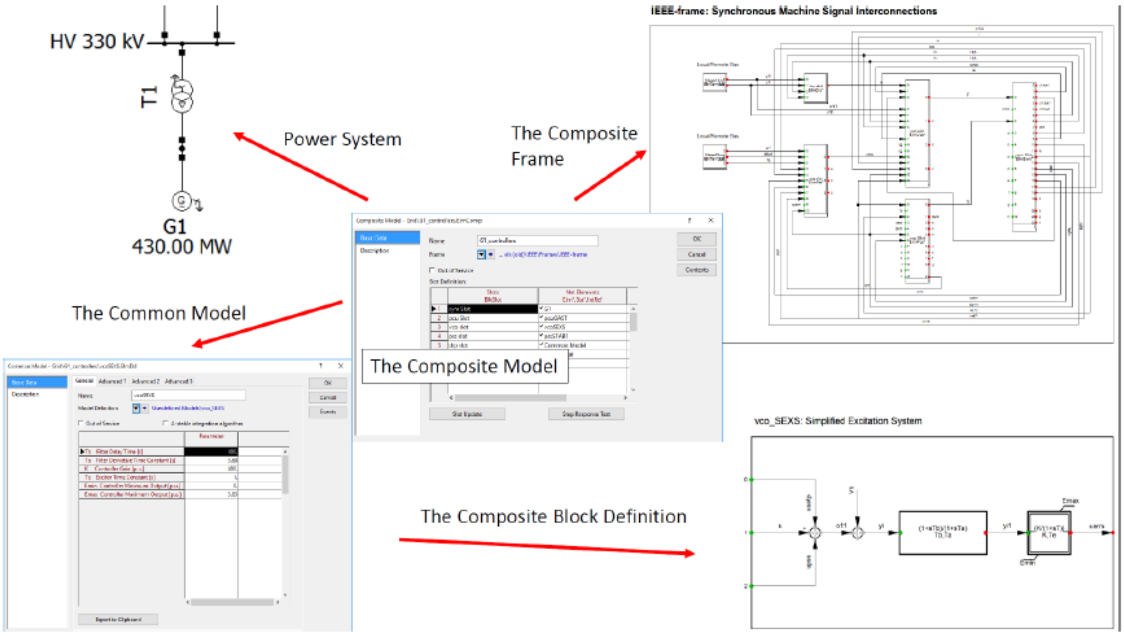


Figure 4.7 Interconnections between 5 elements of modelling in DSL [45]

1. **Power System** – It is a generic model of an electrical system, which contains controllable elements. This element was presented in subchapters 4.1 and 4.2.
2. **Composite Frame** – This schematic represents the input – output relations between different slots. Slots represent controllers or elements of the system (e.g. measurement devices or mechanical elements). The mathematic calculations are not carried in the composite frame.
3. **Block Definition** – This element presents the content of slots presented in a composite frame. It is this element, that holds the control loop and mathematic equations which describes particular element of the system.
4. **Common model** – The equations contained in a block definition often depends on pre-defined parameters (e.g. PI controller block have 2 parameters: proportional gain $K_p$ and integral gain $K_i$). The common model is the table which displays those parameters along with their currently set values. It also allows to change those values

5. **Composite model** – This element displays the table, which elements of Power System or block definitions corresponds with which slots in a composite frame. For example. If in a power system there are 2 voltmeters, but the composite frame holds only one voltmeter slot, then it is defined in the composite model which voltmeter's measured signal is the output signal of voltmeter's slot.

### 4.3.2 Current control model

The inner control loop did not required to be built. The PWM Converter element has an integrated current controller, which is presented in Figure 4.8 [**43**]. The input signals are the *d* and *q* parameters of both measured current and a reference current.. The controllable parameters are the proportional gain *K* and the integration time constant *T* of both PI controllers. The output signals *Pmd* and *Pmq* are the *d* and *q* parameters of pulse width modulation index.

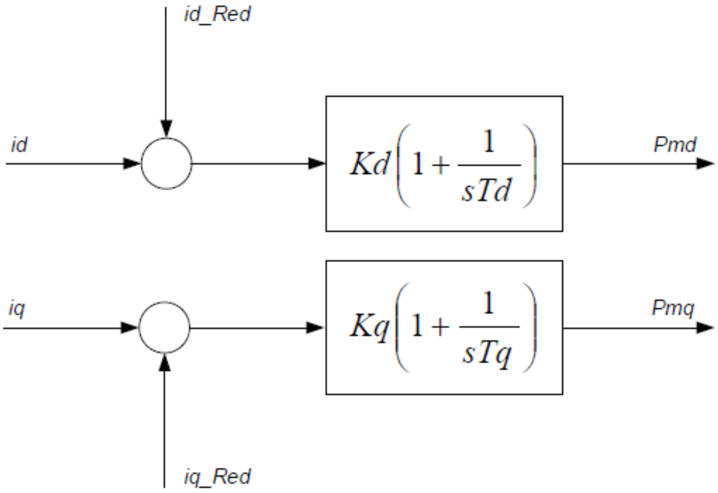


**Figure 4.8 Integrated current controller** [43]

### 4.3.3 P Control Model

The P control is presented in Figure 4.9 and is explained from left to right. The "PQ measurement" block represents the device located at the PCC, which measures active power and send the measurement value as signal. The measured active power is used as an input to "P control" block, that contains the block definition presented in Figure 4.10. The measured powers is subtracted from its reference value and the result signal is sent to a PI controller, which have 2 parameters defined by a user: proportional gain Kp and integral gain Ki. The output signal from "P control" is reference current "id_ref" used as an input signal in an integrated current controller, described in section 4.3.2. The PLL block measures the frequency and the voltage at the PCC, in order to align the grid voltage vector $V_s$ with a *d* axis.

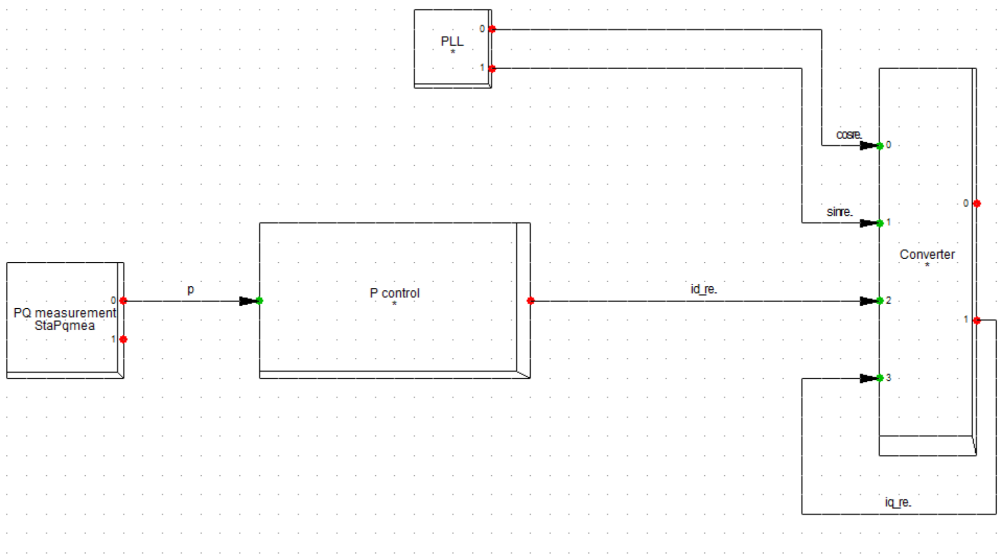


Figure 4.9 P control composite frame

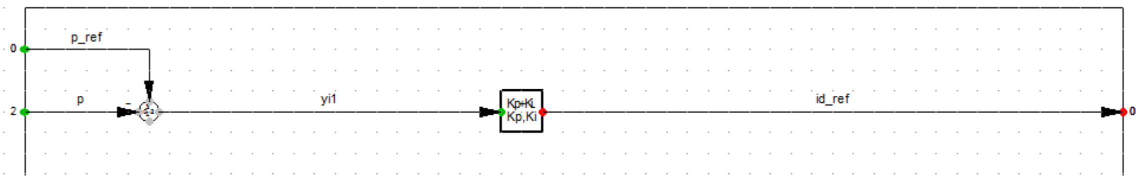


Figure 4.10 P control block definition

### 4.3.4 Udc Control Model

The Udc control is presented in Figure 4.11. The "Udc_n measurement" and the "Udc_p measurement" blocks represents the voltmeters, that measure, respectively, the DC voltage between negative Busbar and the ground, as well as the positive busbar and the ground. Those voltages are sent into the "Udc control" block, which contains a block definition presented in Figure 4.12. Inside the block, the negative voltage is subtracted from the positive voltage. Since voltages are measured in p.u, it is necessary to divide the result of subtraction by 2, in order to keep its value also in p.u. The result voltage is then subtracted from the reference Udc voltage and the result is sent into the PI controller. As in P and Q block, PI controller also have Kp and Ki as predefined parameters. The output of PI controller is the reference current id, sent into the integrated current controller. The PLL block is used in the same way as described in section 4.3.3.

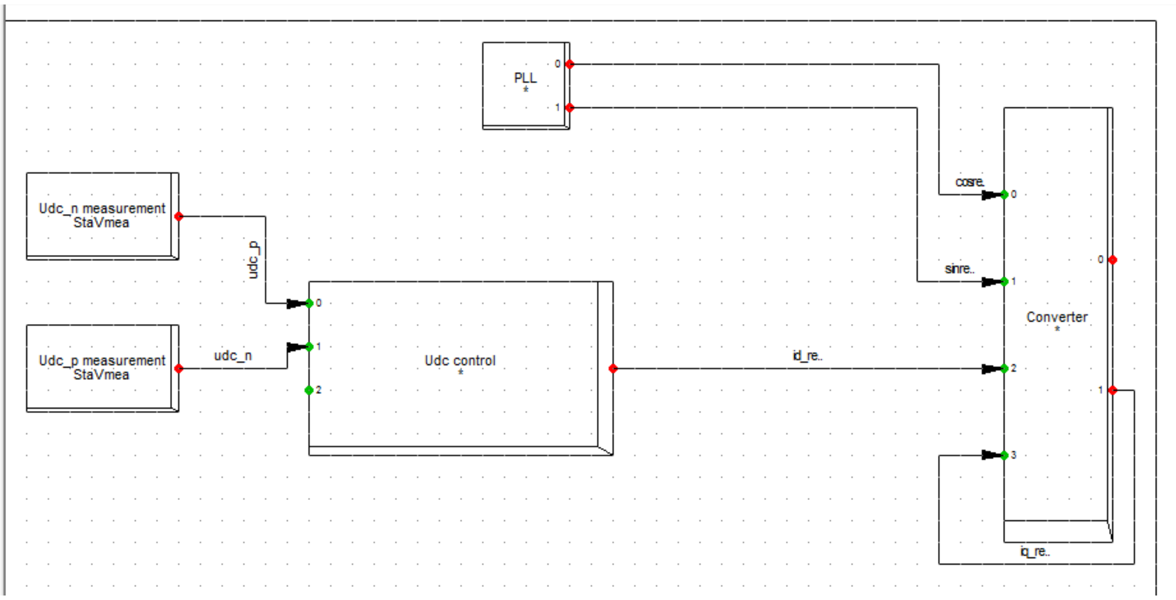


Figure 4.11 Udc control composite frame

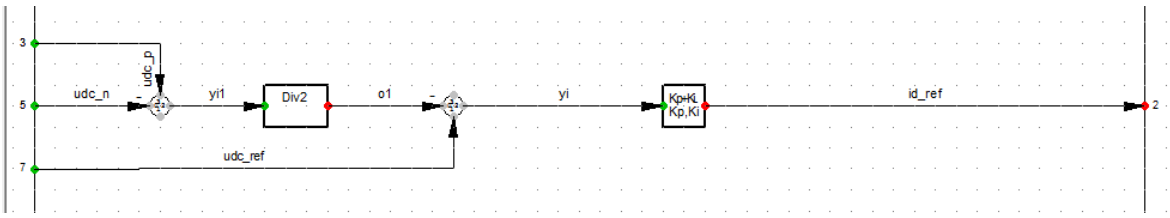


Figure 4.12 Udc control block definition

### 4.3.5 Voltage droop Control Model

The Udc droop control is presented in Figure 4.13. The blocks on the left side represents the P measurement equipment, described in section 4.3.3, and the voltmeters, described in section 4.3.4. The "p" signal and the measured voltages are all used as input for a Udc droop control block, which contains the block definition depicted in Figure 4.14. At the beginning of block definition, signals are processed in the same way as described in previous sections. The difference appear in the middle, where signal that is a result of a measured voltage subtracted from reference voltage is multiplied with a reverse gain 1/K. The K value is a representation of a droop constant "kdc" which is one of the predefined parameters. The result signal is then added to the power subtraction signal, and this signal is sent to a PI controller. From that point, the signal path to controller, the Kp and Ki, and the reason for a PLL block are the same as described in previous sections.

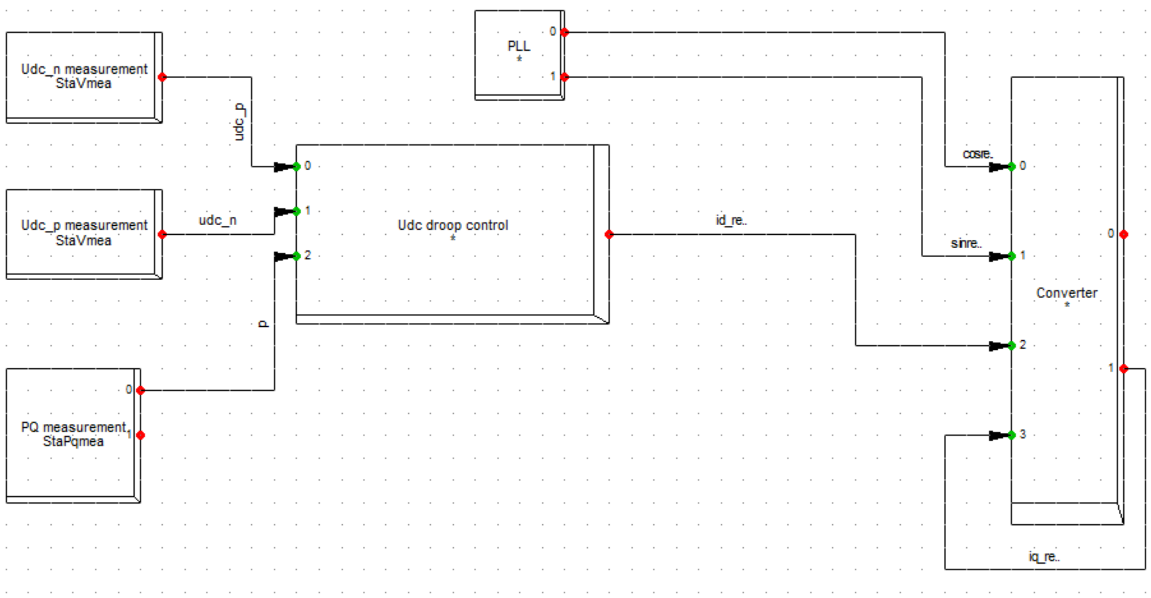


Figure 4.13 Udc droop control frame

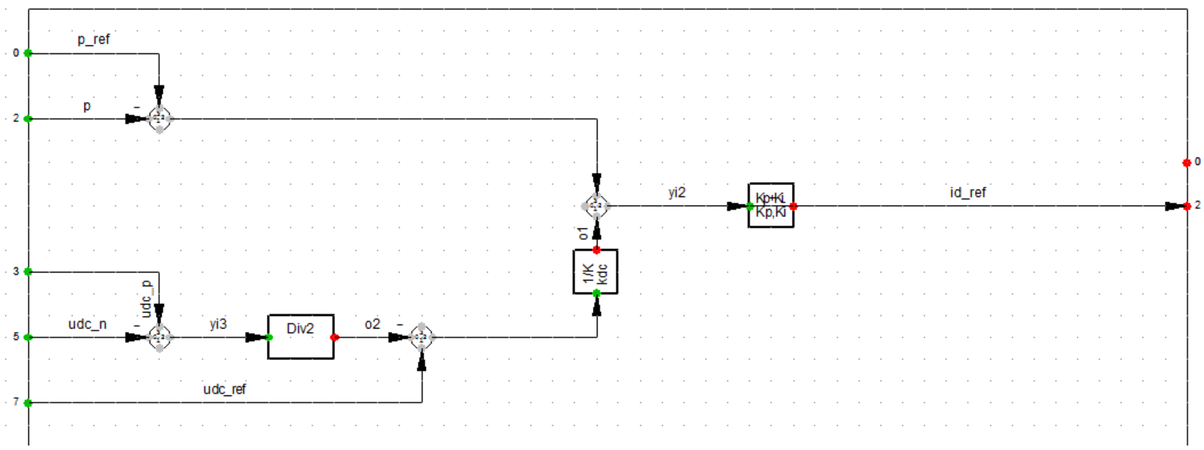


Figure 4.14 Udc droop control block definition

### 4.3.6 Vac-f Control Model

The Vac-f control is depicted in Figure 4.15. This control mode is significantly different than modes presented in previous subchapters. The PWM converter does not have an integrated current controller and the input signals into converter are a magnitude of pulse width modulation and a frequency. In this mode, the measured signals are the DC voltages on DC busbars and the AC voltage on the terminal AC Busbar. All measurements are processed as input signals into the Vac-f control block, which contains the block definition presented in Figure 4.16. The reference frequency and the reference AC voltage are not controllable, they are constant value s implemented as parameters. This situation is caused by a fact that the behaviour of the AC system connected to wind farm is not in the scope of this project. The measured AC voltage is subtracted from the reference voltage and then processed to a PI controller, with Kp and Ki as predefined parameters. The resulted as voltage is processed to a “Pm calculation block”, which second input signal is a measured DC voltage. In this block, the Pm is calculated based on equation 4.3 [**43**]. The calculated Pm and constant frequency are than processed to the converter.

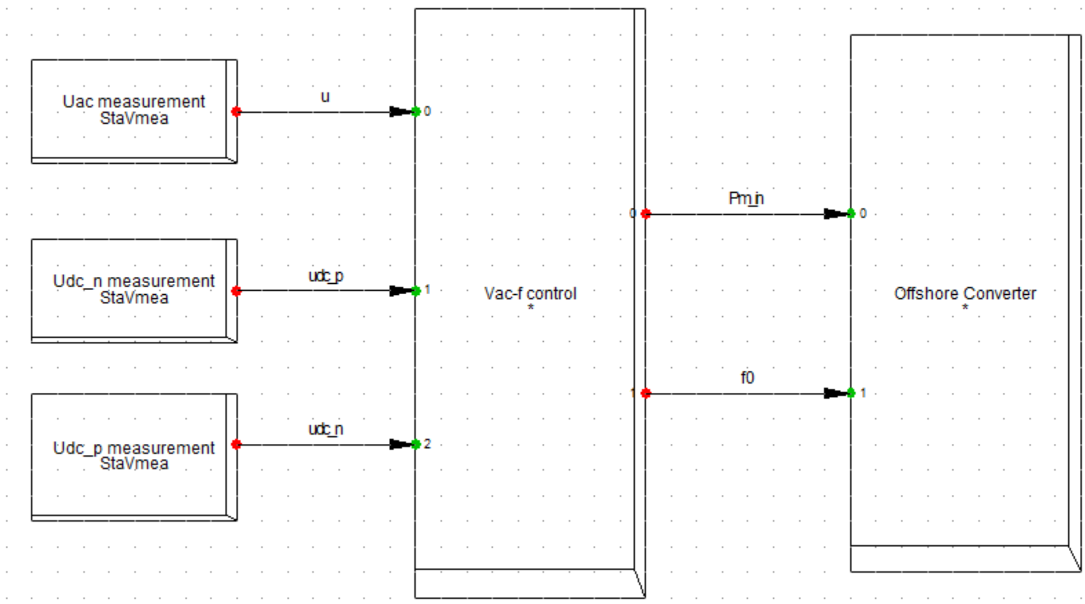


Figure 4.15 Vac-f control frame

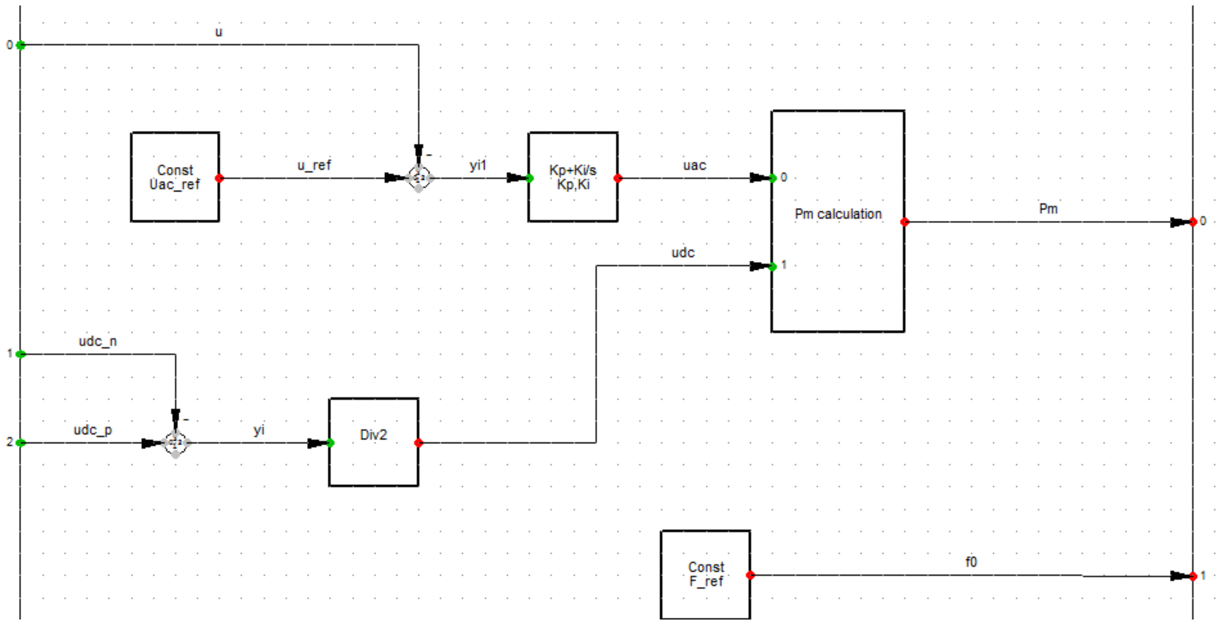


Figure 4.16 Vac-f control block definition

$$P_m = \frac{2 \cdot \sqrt{2} \cdot U_{AC}}{\sqrt{3} \cdot U_{DC}} \quad 4.3$$

# 5. Analyses of the system

The control modes presented in subchapter 4.3 have been implemented into the generic models presented in subchapters 4.1 and 4.2. Since no errors were reported by DIgSILENT Power Factory, the next step was supposed to be tuning the PI controllers and performing analyses presented in the problem statement. Due to lack of time necessary to complete those analyses, only the methodology is presented.

## 5.1 PI Controllers Tuning

All PI controllers which were implemented in the control modes models need to be tuned prior to testing the behaviour of MTDC system. The tuning process was supposed to be carried by a trial and error method on a PtP connection generic model.

### 5.1.1 Current Controller Tuning

Since the “iq” control is out of the project scope, the “Tq” parameter is set to 0, which makes “iq” always equal to “iq_ref” [**43**]. As for PI controller for “id” control, it have to be tuned according to changes in both “id” and “id_ref” signals. The tuning was supposed to be carried on a PtP model with a “P control” implemented as a control mode in the first converter and the “Udc control” implemented in the second converter. The bandwidth in which the controller is stable was supposed to be found by putting a 100 ms short circuit event at the AC terminal of a VSC and measure the “id” signal response. The values of “Kd” and “Td” that result in optimal system response were supposed to be found by changing the “id_ref” value from 1 p.u to 0.9 p.u. Based on two described tests, the values of “Kd” and “Td” that should be implemented in a PI controller are the values inside the stability bandwidth which are closest to those resulting in an optimal system response.

### 5.1.2 P Controller Tuning

Tuning of PI controller in P control was supposed to be done in the same PtP model in which the Current controller was tuned. Tuning process should be done in a similar manner, with regards to changes in both “p” and “p_ref” signals. The bandwidth in which the controller is stable was supposed to be found by putting a 100 ms short circuit event at the AC terminal of a VSC and measure the “p” signal response. The values of “Kp” and “Ki” that result in an optimal system response were supposed to be found by changing the “p_ref” value from 1 p.u to 0.9 p.u. Based on those tests, the values of “Kp” and “Ki” that should be implemented in a PI controller are the values inside the stability bandwidth which are closest to those resulting in an optimal system response.

### 5.1.3 Udc Controller Tuning

Tuning of PI controller in Udc control was supposed to be done in the same PtP model in which the Current controller a P controller were tuned. Tuning process should be done in a similar manner, with regards to changes in both “udc” and “udc_ref” signals. The bandwidth in which the controller is stable was supposed to be found by putting a 100 ms short circuit event at the AC terminal of a VSC and measure the “udc” signal response. The values of “Kp” and “Ki” that result in an optimal system response were supposed to be found by changing the “udc_ref” value from 1 p.u to 0.98 p.u. Based on those tests, the values of “Kp” and “Ki” that should be implemented in a PI controller are the values inside the stability bandwidth which are closest to those resulting in an optimal system response.

### 5.1.4 Voltage Droop Controller Tuning

Tuning of a PI controller in Udc droop control was supposed to be done in an MTDC model in which first converter is set into “ Udc droop control” mode, the second converter mode is “P control” and the windfarm operates in “Vac-f”. Tuning process should be done with regards to changes in “udc”, “udc_ref”, “p”, “p_ref” signals and the value of a droop constant “kdc”. The bandwidth in which the controller is stable was supposed to be found by putting a 100 ms short circuit event at the AC terminal of a VSC and measure the output signal “id_ref” response. The values of “Kp” and “Ki” that result in an optimal system response were supposed to be found by changing either the “udc_ref” value or “p_ref” value. Based on those tests, the values of “Kp” and “Ki” that should be implemented in a PI controller are the values inside the stability bandwidth which are closest to those resulting in an optimal system response. After that, the tuned PI droop controller would be implemented in an MTDC model where control mode of second converter would be changed from “P control” to “Udc control”, in order to check if in this configuration the PI controller requires different “Kp” and “Ki” parameters for optimal response.

### 5.1.5 Vac-f Controller Tuning

The PI controller in this mode would be tuned on an MTDC model, with first converter set into “P control” and second converter set into “Udc control” Since “Vac_ref” and reference frequency are constant, only 100 ms short circuit would be implemented to determine the stability bandwith.

## 5.2 System behaviour

The tuned PI controller's values would be implemented into 3 types of an MTDC dispatch control model, that is:

1. Master-slave method – One converter operates in Udc control, one in PQ control and the windfarm converter in an Vac-f control.
2. Udc droop method – Both Danish and Netherland's converters set into droop control, windfarm converter operates in Vac-f control.
3. Master-slave with droop control – One converter operates in Udc control, one in droop control and windfarm converter in Vac-f mode.

For all 3 of dispatch controls mentioned above, the tests described in sections 5.2.1 to 5.2.3 would be performed. In all of them, the following signals would be measured at every converter:

- Transferred Active Power
- Transferred Reactive Power
- DC Voltage
- DC Current
- AC Voltage

### 5.2.1 Three phase short circuit

In this situation, a 100 ms short circuit would occur at every converter, one SC at a time, and the response of every converter would be compared in order to determine the most reliable dispatch control in terms of SC occurrence.

### 5.2.2 Reduced Power Transfer

In normal condition, offshore wind farm generates 700 MVA, which is distributed equally into Danish and Netherlands grid. In this test, the wind farm generation would drop to 350 MVA. The signals would be compared in order to determine which dispatch strategy is the best for this type of situation.

### 5.2.3 Loss of converter

In this test, every converter would be shut down and disconnected from a grid due to a fault, one converter at a time. The measured signals would be compared in order to determine which strategy ensures the fastest recovery of 2 remaining converters.

## 5.3 Sensitivity Analisys

The final test in the project would determine how sensible the MTDC grid is, based on changes in an inner current controller PI, outer control mode PI and the droop constant. It would also be checked if the PI controller values determined in subchapter 5.1 are still resulting In the best possible performance, or does controllers may be re-tuned to achieve better response.

# 6. Conclusions and Future work

The problem statement in the project has remained unsolved due to lack of time necessary for finishing the project. However, the DigSILENT model is fully operational and the methodology for performing the analyses described in chapter 5 is known, thus only time is required in order complete the project.

## 6.1 Future work

Regardless of inability to complete a project, a few suggestions for future work were concluded:

- The MTDC grid should be expanded in the future to connect more terminals, in order to determine how the number of terminals affects the parameters.
- The Q control should be included in the control modes
- The created control modes models may be improved (e.g. with filters)
- The performance analysis may also include lower control
- Implementation of classified COBRAcable data into the model will result in more realistic results
- The function how kdc affects optimal Kp and Ki gains in a droop control strategy may be determined

# References


[1] Commission of the European Communities, "AN EU ENERGY SECURITY AND SOLIDARITY ACTION PLAN," Brussel, 2008.

[2] The European Wind Energy Association, "The European offshore wind industry - key trends and statistics 2014," 2015.

[3] Stjin Cole, Pierre Martinot, Stephane Rapoport, Georgios Papaefthymiou, and Valerio Gori, "STUDY OF THE BENEFITS OF A MESHED OFFSHORE GRID IN NORTHERN SEAS REGION - Final Report," 2014.

[4] "Political declaration on the North Seas Countries Offshore Grid Initiative," 2009.

[5] "The North Seas Countries Offshore Grid Initiative - Memorandum of Understanding," 2010.

[6] (2015) Benelux General Secretariat. [Online]. http://www.benelux.int/nl/kernthemas/energie/nscogi-2012-report/

[7] Working Group 1 – Grid Configuration, "The North Seas Countries' Offshore Grid Initiative Initial Findings," 2011.

[8] Roni Irnawan, Filipe Faria da Dilva, and Claus Leth Bak, "A Categorization of Converter Station Controllers Within Multi-terminal DC Transmission Systems,".

[9] (2016) TenneT website. [Online]. http://www.tennet.eu/nl/grid-projects/international-projects/cobracable.html

[10] (2016) Energinet.dk website about COBRAcable. [Online]. http://www.energinet.dk/EN/ANLAEG-OG-PROJEKTER/Anlaegsprojekter-el/Kabel-til-Holland-COBRA/Sider/Kabel-til-Holland-COBRA.aspx

[11] ABB. (2015, september) HVDC - ABB Technology guide. [Online]. http://www.abb.com/cawp/db0003db002698/9662333421d49f15c1257203006472d4.aspx

[12] Ryan Hamerly. (2015, september) Student technical information. [Online]. http://web.stanford.edu/~rhamerly/cgi-bin/Ph240/Ph240-1.php

[13] Teshmont, "HVDC PROJECTS LISTING," 2012.

[14] ABB. (2015, september) ABB review - HVDC special report. [Online]. http://new.abb.com/systems/hvdc

[15] Asplund Gunnar, Eriksson Kjell, and Svenson Kjell, "DC Transmission based on Voltage Source Converters," , 1997.

[16] Carsten Rasmussen, "Supply of Copenhagen/132 kV grid in Copenhagen," , Kolding, 2015.

[17] Siemens, "Fact Sheet: High-voltage direct current transmission (HVDC)," 2012.

[18] RL Sellick and M Åkerberg, "Comparison of HVDC Light (VSC) and HVDC Classic (LCC) Site Aspects, for a 500MW 400kV HVDC Transmission Scheme," , Birmingham, 2012.

[19] Persson Gunnar, "HVDC Converter Operations and Performance, Classic and VSC," , Dhaka, 2011.

[20] Siemens, "High Voltage Direct Current Transmission – Proven Technology for Power Exchange," 2011.

[21] Xiaobo Yang, Chunming Yuan, Dawei Yao, Chao Yang, and Chengyan Yue, "Dynamic performance of series multiterminal HVDC during AC faults at inverter stations," in *Energy and Power Engineering*, Lappeenranta, 2014.

[22] European Network of Transmission System Operators for Electricity, "Offshore Transmission Technology," , 2011.

[23] Caroline Kamerbeek. (2014) DNV GL Energy news. [Online]. https://www.dnvgl.com/news/dnv-gl-advises-on-world-s-first-multi-terminal-vsc-hvdc-transmission-project-integrating-clean-energy-into-china-s-regional-power-composition-mix-6205

[24] Oriol Gomis-Bellmunta, Jun Liang, Janaka Ekanayake, Rosemary King, and Nicholas Jenkins, "Topologies of multiterminal HVDC-VSC transmission for large offshore wind farms," *Electric Power Systems Research*, no. 81, pp. 271-281, 2011.

[25] Cigre. (2015, september) OVERVIEW OF LINE COMMUTATED CONVERTER BASED, HVDC. [Online]. http://b4.cigre.org/content/download/1971/25259/version/1/file/What+is+HVDCID10VER33.pdf

[26] Sanjay Chaudhary, "Graetz bridge Converters and LCC HVDC - presentation in "High Power Converters" course,".

[27] Siemens, "Harmonics in power systems - Causes, effects and control," , 2013.

[28] Stephen Lagakos et al., *Recent Advances in Circuits, Systems, Signal and Telecommunications*. Cambridge, USA, 2010.

[29] Cui-Qin Dai, M.H.J. Bollen, E. Agneholm, and A. Sannino, "A New Control Strategy of a VSC–HVDC System for High-Quality Supply of Industrial Plants," vol. 22, no. 4, 2007.

[30] Shri Harsha J, Shilpa G N, Ramesh E, Dayananda L N, and Nataraja.C, "Voltage Source Converter Based HVDC Transmission," vol. 1, no. 1, 2012.

[31] Nikolas Flourentzou, Vassilios G. Agelidis, and Georgios D. Demetriades, "VSC-Based HVDC Power Transmission Systems: An Overview," vol. 24, no. 3, 2009.

[32] Amirnaser Yazdani and Reza Iravani, *VOLTAGE-SOURCED CONVERTERS IN POWER SYSTEMS: Modeling, Control, and Applications*. New Jersey, USA: John Wiley & Sons, Inc., 2010.

[33] Ned Mohan, Tore Undeland, and William Robbins, *POWER ELECTRONICS Converters, Applications and Design*, 2nd ed. New York: John Wiley & Sons.Inc, 1995.

[34] Temesgen Mulugeta Haileselassie, "Control, Dynamics and Operation of Multi-terminal VSC-HVDC Transmission Systems," Norwegian University of Science and Technology, Trondheim, Thesis for the degree of Philosophiae Doctor 2012.

[35] Siemens, "HVDC PLUS – Basics and Principle of Operation," Technical Report 2011.

[36] Carlos Castillo Bonilla and Shweta Merilyn Tigga, "Design and performance comparison of Two-level and Multilevel Converters for HVDC Applications," CHALMERS UNIVERSITY OF TECHNOLOGY, Göteborg, Master's Thesis in Electric Power Engineering 2011.

[37] Radnya A Mukhedkar, "Introduction to HVDC - LCC & VSC - Comparison,".

[38] Working Group B4.57, "Guide for the Development of Models for HVDC Converters in a HVDC Grid," CIGRE, 2014.

[39] Mike Barnes and Antony Beddard, "Voltage Source Converter HVDC Links – The state of the Art and Issues Going Forward," *Energy Procedia*, vol. 24, pp. 108-122, 2012.

[40] Kaiyuan Lu, "Dynamic modeling of electric machines," , Materials from the course held in Aalborg University in Autumn 2014.

[41] Lidong Zhang, Lennart Harnefors, and Hans-Peter Nee, "Power-Synchronization Control of Grid-Connected Voltage-Source Converters," *IEEE Transactions on Power Systems*, vol. 25, no. 3, pp. 809 - 820, November 2009.

[42] DIgSILENT PowerFactory, "HVDC Connected Offshore Wind Farm," A PDF file which describes an example of HVDC offshore windfarm.

[43] DIgSILENT PowerFactory, "Technical Reference," PDF documents regarding technical description of elements from Power Factory.

[44] ABB, "It's time to connect," 2012.

[45] DIgSILENT PowerFactory, "User Manual,".